TECHNICAL MEMORANDUMS

NATIONAL ADVISORY COMMITTEE FOR AERONAUTICS

No. 884

CALCULATION OF THE INDUCED EFFICIENCY OF HEAVILY LOADED PROPELLERS HAVING INFINITE NUMBER OF BLADES

By F. Lösch

THE INDUCED EFFICIENCY OF OPTIMUM PROPELLERS HAVING A FINITE NUMBER OF BLADES

By K. N. Kramer

PROSPECTS OF PROPELLER DRIVE FOR HIGH FLYING SPEEDS

By G. Bock and R. Nikodemus

Luftfahrtforschung
Vol. 15, No. 7, July 6, 1938
Verlag von R. Oldenbourg, München und Berlin

Washington
January 1939

NATIONAL ADVISORY COMMITTEE FOR AERONAUTICS

TECHNICAL MEMORANDUM NO. 884

CALCULATION OF THE INDUCED EFFICIENCY OF HEAVILY LOADED PROPELLERS HAVING INFINITE NUMBER OF BLADES*

By F. Lösch

SUMMARY

Based on a suggestion made by L. Prandtl, the present report contains an approximate method of computing the induced efficiency of heavily loaded propellers in suitable form for extension to finite number of blades, and a comparison of the results obtained by this simple method with the data of the Betz-Helmbold theory for heavily loaded propellers. It is found that - quite apart from the accord in the limiting case of light loading - good agreement obtains for relatively low as for relatively high coefficients of advance. A direct calculation of the (c_s, η_i) curves by the two methods affords excellent agreement up to $\eta_i = 0.5$, even for ~~efficiences~~ λ's in the neighborhood of 0.5, 1, 2.

Notation

ρ, air density

R, propeller radius

r, distance of any propeller element from the axis

$x = \frac{r}{R}$, nondimensional radial coordinate of any propeller element

$F_p = \pi R^2$, swept-disk area of propeller

ϵ_p, lift-drag ratio of profile

ω_p, angular velocity

---

*"Über die Berechnung des induzierten Wirkungsgrads stark belasteter Luftschrauben unendlicher Blattzahl." Luftfahrtforschung, vol. 15, no. 7, July 6, 1938, pp. 321-325.

$u = R\,\omega_p$, tip speed

v, velocity of advance

$\lambda = \dfrac{v}{u}$, coefficient of advance

w, impact velocity

$\vartheta = \dfrac{w}{v}$, slip

$\beta = \operatorname{arc\,tan} \dfrac{v}{r\,\omega_p}$, angle of advance

$\beta_i = \operatorname{arc\,tan} \dfrac{v + \frac{1}{2} w}{r\,\omega_p}$, induced angle of advance

$\frac{1}{2} w_a$, axial component of the interference velocity at the blade

$\frac{1}{2} w_t$, tangential component of the interference velocity at the blade

$\frac{1}{2} w_n = \sqrt{\left(\frac{1}{2} w_a\right)^2 + \left(\frac{1}{2} w_t\right)^2}$, total interference velocity at the blade

$S = \frac{1}{2} c_s\,\rho\,v^2\,F_p$, thrust

$N = \frac{1}{2} c_l\,\rho\,v^3\,F_p$, ~~performance~~ power

c_s, coefficient of thrust loading

c_l, coefficient of power loading

$\eta_i = \dfrac{c_s}{c_l}$ for $\epsilon_p = 0$, induced efficiency

$\lambda_i = \dfrac{\lambda}{\eta_i}$, induced coefficient of advance

$\Gamma^{(\infty)} \equiv \Gamma^{(\infty)}_{(r)}$, total circulation about the blade sections at distance r from the axis

$\underline{G}^{(\infty)} = \dfrac{1}{2\,\pi\left(1 + \frac{\vartheta}{2}\right)} \dfrac{\omega_p}{v\,w}\,\Gamma^{(\infty)} = \dfrac{x^2}{x^2 + \lambda_i^{\,2}}$, nondimensional circulation distribution

$$K_{m,n}^{(\infty)} \equiv K_{m,n}^{(\infty)}(\lambda_i) = \int_0^1 \frac{x^m}{(x^2 + \lambda_i^2)^n} dx$$

1. INTRODUCTION

Visualize a propeller of "infinite" blade number moving with coefficient of advance λ in a free stream. Let c_s and c_l, respectively, denote its thrust loading and power loading computed for vanishing profile lift/drag ratio ϵ_p so that $\eta_i = \frac{c_s}{c_l}$ is its induced efficiency. The problem in the following involves the solution of the relationship between η_i, c_s, and λ for the case of heavy loading. Thereby it is assumed that the propeller is an "optimum" propeller in the usual sense, i.e., produces a given thrust with least possible energy loss.

2. APPROXIMATE METHOD OF COMPUTING THE INDUCED EFFICIENCY ACCORDING TO L. PRANDTL

One approximate method for computing the desired relationship between η_i, c_s, and λ ties in with the case of light loading. In this case the flow sufficiently downstream from a propeller having minimum energy loss is, according to Betz (reference 1, pp. 69-70), as if the path covered by each propeller blade (a helical surface whose pitch at distance r from the axis is given by the angle of advance $\beta = \text{arc tan} \frac{v}{r\omega_p}$) had congealed and shifted backward at a definite velocity, called the impact velocity w (fig. 1). On the basis of this theorem, the interference velocity at the blade can be computed in the following known manner (cf. reference 1, pp. 88-89):

Since Betz's so-called helical surfaces lie close together on the propeller of infinite blades, the interferference velocities are axially symmetrical in respect to the axis of the slipstream, that is, their magnitude depends solely upon the distance r from the axis. Moreover, the interference velocities are perpendicular to the helical surfaces created by their displacement at velocity w (as a result of which the radial component of the interference velocity, particularly, disappears). Besides, since, owing to the light loading, the slipstream contraction can be ignored, the interference velocities in the swept-disk area are half as great as in the developed slipstream. Therefore, if $\frac{1}{2} w_a$ indicates the axial component, $\frac{1}{2} w_t$ the tangential component, and $\frac{1}{2} w_n$ the total interference velocity at the blade, the components at distance r from the axis can be expressed (as shown in figure 2) by w as follows:

$$\frac{1}{2} w_n = \frac{1}{2} w \cos \beta$$

hence:

$$\frac{1}{2} w_a = \frac{1}{2} w_n \cos \beta = \frac{1}{2} w \cos^2 \beta$$

$$\frac{1}{2} w_t = \frac{1}{2} w_n \sin \beta = \frac{1}{2} w \sin \beta \cos \beta$$

and, as a result of $\tan \beta = v/r\,\omega_p$

$$\frac{1}{2} w_a = \frac{1}{2} w \frac{(r\,\omega_p)^2}{v^2 + (r\,\omega_p)^2}, \quad \frac{1}{2} w_t = \frac{1}{2} w \frac{v(r\,\omega_p)}{v^2 + (r\,\omega_p)^2} \qquad (1)$$

or, after introduction of the nondimensional radial coordinate $x = \frac{r}{R}$,

$$\frac{1}{2} w_a = \frac{1}{2} w \frac{x^2}{x^2 + \lambda^2}, \quad \frac{1}{2} w_t = \frac{1}{2} w \frac{x\,\lambda}{x^2 + \lambda^2} \qquad (2)$$

According to a remark by L. Prandtl (reference 1, p. 89) the foregoing formulas afford a practical approximation for the interference velocities on moderately loaded propellers, when v is replaced by $v + \frac{1}{2} w$, through which the induced angle of advance $\beta_i = \arc\tan \frac{v + \frac{1}{2} w}{r\,\omega_p}$ takes the place of the angle of advance β (fig. 3). Then equations (1) read:

$$\left.\begin{aligned} \frac{1}{2} w_a &= \frac{1}{2} w \frac{(r\,\omega_p)^2}{\left(v + \frac{1}{2} w\right)^2 + (r\,\omega_p)^2} \\ \frac{1}{2} w_t &= \frac{1}{2} w \frac{\left(v + \frac{1}{2} w\right) r\,\omega_p}{\left(v + \frac{1}{2} w\right)^2 + (r\,\omega_p)^2} \end{aligned}\right\} \qquad (3)$$

or, after introducing x and the slip $\vartheta = \frac{w}{v}$,

$$\left.\begin{aligned} \frac{1}{2} w_a &= \frac{1}{2} w \frac{x^2}{x^2 + \lambda^2 \left(1 + \frac{\vartheta}{2}\right)^2} \\ \frac{1}{2} w_t &= \frac{1}{2} w \frac{x \lambda \left(1 + \frac{\vartheta}{2}\right)}{x^2 + \lambda^2 \left(1 + \frac{\vartheta}{2}\right)^2} \end{aligned}\right\} \qquad (4)$$

From these equations both the thrust and the performance are directly obtainable by the Kutta-Joukowski theorem. The total circulation about all propeller elements at equal distance r from the axis is:

$$\Gamma^{(\infty)} \equiv \Gamma^{(\infty)}_{(r)} = 2\,\pi\,r\,w_t$$

and the ensuing elements of the axial and tangential force acting on the propeller are:

$$d\,S = \rho\,\Gamma^{(\infty)}\left(r\,\omega_p - \frac{1}{2}\,w_t\right) d\,r = 2\pi\,\rho\,r\,w_t\left(r\,\omega_p - \frac{1}{2}\,w_t\right) d\,r$$

$$d\,T = \rho\,\Gamma^{(\infty)}\left(v + \frac{1}{2}\,w_a\right) d\,r = 2\,\pi\,\rho\,r\,w_t\left(v + \frac{1}{2}\,w_a\right) d\,r$$

These expressions, when written in equation (4) followed by integration of $d\,S$ and $r\,\omega_p\,d\,T$ over the whole propeller; i.e., after introduction of x over x from 0 to 1, give the thrust and performance as:

$$S = \int_0^R d\,S = \frac{\rho}{2}\,\pi\,v^2\,R^2\left[4\,\vartheta\left(1 + \frac{\vartheta}{2}\right)\int_0^1 \underline{G}^{(\infty)}\,x\,d\,x - 2\,\vartheta^2\int_0^1 \underline{G}^{(\infty)}\,\frac{x\,\lambda^2\left(1 + \frac{\vartheta}{2}\right)^2}{x^2 + \lambda^2\left(1 + \frac{\vartheta}{2}\right)^2}\,d\,x\right] \tag{5}$$

$$N = \int_0^R r\,\omega_p\,d\,T = \frac{\rho}{2}\,\pi\,v^3\,R^2\left[4\,\vartheta\left(1 + \frac{\vartheta}{2}\right)^2\int_0^1 \underline{G}^{(\infty)}\,x\,d\,x - 2\,\vartheta^2\left(1 + \frac{\vartheta}{2}\right)\int_0^1 \underline{G}^{(\infty)}\,\frac{x\,\lambda^2\left(1 + \frac{\vartheta}{2}\right)^2}{x^2 + \lambda^2\left(1 + \frac{\vartheta}{2}\right)^2}\,d\,x\right] \tag{6}$$

where $\underline{G}^{(\infty)}$ denotes the nondimensional circulation distribution

$$\underline{G}^{(\infty)} = \frac{1}{2\,\pi\left(1 + \frac{\vartheta}{2}\right)}\,\frac{\omega_p}{v\,w}\,\Gamma^{(\infty)} = \frac{x^2}{x^2 + \lambda^2\left(1 + \frac{\vartheta}{2}\right)^2}$$

The induced efficiency follows direct from equations (5) and (6) as:

$$\eta_i = \frac{c_s}{c_l} = \frac{S v}{N} = \frac{1}{1 + \frac{\vartheta}{2}} \tag{7}$$

or inversely the slip expressed by the efficiency

$$\vartheta = \frac{2(1 - \eta_i)}{\eta_i} \tag{8}$$

With regard to Kramer's application (reference 3) in the following, it is recommended to transform the expression (equation (5)) for the thrust. To this end the induced coefficient of advance $\lambda_i = \frac{\lambda}{\eta_i}$ is introduced and a notation patterned after Helmbold, is posed:

$$K_{m,n}^{(\infty)} \equiv K_{m,n}^{(\infty)} (\lambda_i) = \int_0^1 \frac{x^m}{(x^2 + \lambda_i^2)^n} d x \quad (m, n \text{ whole, positive}) \tag{9}$$

These integrals obviously comply with the relation

$$K_{m+2,n+1}^{(\infty)} = K_{m,n}^{(\infty)} - \lambda_i^2 K_{m,n+1}^{(\infty)} \tag{10}$$

With this notation we find:

$$\int_0^1 \underline{G}^{(\infty)} x d x = \int_0^1 \frac{x^3}{x^2 + \lambda_i^2} d x = K_{31}^{(\infty)}$$

$$\int_0^1 \underline{G}^{(\infty)} \frac{x \lambda^2 \left(1 + \frac{\vartheta}{2}\right)^2}{x^2 + \lambda^2 \left(1 + \frac{\vartheta}{2}\right)^2} d x = \int_0^1 \frac{\lambda_i^2 x^3}{(x^2 + \lambda_i^2)^2} d x = \lambda_i^2 K_{32}^{(\infty)}$$

and introduced in equation (5) while allowing for

$$K_{31}^{(\infty)} - \lambda_i^2 \; K_{32}^{(\infty)} = K_{52}^{(\infty)}$$

applicable by virtue of equation (10),

$$c_s = \frac{S}{\frac{\rho}{2} \pi R^2 v^2} = 4 \; \vartheta \; K_{31}^{(\infty)} + 2 \; \vartheta^2 \; K_{52}^{(\infty)} \tag{11}$$

The elimination of ϑ from equations (8) and (11) leaves the desired relationship between η_i, c_s, and λ. The evaluation of integrals $K_{31}^{(\infty)}$ and $K_{52}^{(\infty)}$ gives

$$K_{31}^{(\infty)} = \frac{1}{2} \left[1 - \lambda_i^2 \ln \left(1 + \frac{1}{\lambda_i^2} \right) \right],$$

$$K_{52}^{(\infty)} = \frac{1}{2} \left[1 - 2 \; \lambda_i^2 \; \ln \left(1 + \frac{1}{\lambda_i^2} \right) + \frac{\lambda_i^2}{1 + \lambda_i^2} \right]$$

which, when written into equation (11) along with ϑ from equation (8), gives:

$$c_s = \frac{4(1 - \eta_i)}{\eta_i^2} \left[1 - (2 - \eta_i) \; \lambda_i^2 \; \ln \left(1 + \frac{1}{\lambda_i^2} \right) + (1 - \eta_i) \frac{\lambda_i^2}{1 + \lambda_i^2} \right] \tag{12}$$

3. METHOD OF COMPUTING THE INDUCED EFFICIENCY ACCORDING TO BETZ-HELMBOLD

Betz and Helmbold (reference 2) have developed a theory for the heavily loaded propeller which allows for the slipstream contraction. The relationship between thrust and efficiency for the best propeller according to their theory is as follows*:

---

*To preserve the modern standards of symbols, the notation used hereinafter differs from that employed in the Betz-Helmbold report; particularly, the radii and velocities relating to the developed jet are denoted with a dash, while on the corresponding quantities relating to the propeller circle the dash has been omitted.

With the customary optimum consideration for the lightly loaded propeller, it is found first of all that the most favorable thrust grading is obtained if a small increase in thrust is produced by a corresponding circulation increase at every point of the propeller with the same efficiency. This also holds for heavy loading.

In the case of lightly loaded propeller, the effect on the slipstream is the same ~~as~~ if this supplementary thrust ~~were~~ was applied at a point of the propeller circle itself or at a corresponding point of the slipstream. The latter offers the advantage of invalidating the reaction of the thrust ~~augmenter~~ increment on the rest of the propeller, and it leaves a simple condition for the interference velocity in the developed slipstream and hence for the thrust grading.

In the case of a heavily loaded propeller, on the other hand, the shifting of the thrust ~~augmenter~~ increment into the slipstream is not summarily admissible. For, now an increase in circulation and hence of the thrust at any point $r = r_0$ of the propeller circle, results in increased axial flow velocity at the propeller circle, once at point $r = r_0$ itself, and then, on account of the increased jet rotation and the engendered rise in positive pressure in the jet, on the entire disk area $r \leqq r_0$; consequently, more fluid streams through the propeller circle than before the circulation rise. Contrariwise, applying the same circulation rise at a corresponding point of the slipstream again results in increased axial flow velocity, but now, since the amount of flow is given by the far upstream propeller circle, on which nothing is changed, it effectuates a supplementary jet contraction. Hence, in order to obtain the same developed jet and so the same thrust as with the circulation rise at the propeller circle, the circulation increase which effects a supplementary thrust ΔS_1 must be accompanied by an increase in jet, which involves a further supplemental thrust ΔS_2. Then, observing that the effect of the jet increase ΔS_2 is proportional to the supplementary thrust ΔS_1, we obtain as thrust increase, which corresponds to the questioned circulation increase at the propeller circle itself,

$$\Delta S = \Delta S_1 + \Delta S_2 = C \Delta S_1$$

with $C > 1$.

In the Betz-Helmbold theory, the decisive assumption is made that C is unaffected by the radius r at which the supplementary thrust is applied. It is shown that this can be realized by suitable (probably fairly little) curvature of the swept-disk area. On these premises, the optimum consideration can be carried on in the same manner as for the lightly loaded propeller. Denoting with R' the radius of the developed slipstream and with w_a' and w_t', respectively, the axial and tangential component of the interference velocity in the jet solely dependent upon the distance r' from the axis, the condition reads

$$\frac{v(r'\omega_p - w_t')}{r'\omega_p(v + w_a')} = \eta_1 \tag{13}$$

with $\eta_1 < 1$ unrelated to r'. Introducing the auxiliary quantities constant with η_1 also over the total jet radius

$$v_1 = \frac{v}{\eta_1}, \quad w_1 = v_1 - v, \quad \vartheta_1 = \frac{w_1}{v} \tag{14}$$

equation (13) can be written in the form

$$\frac{v + w_a'}{r'\omega_p - w_t'} = \frac{v_1}{r'\omega_p} = \frac{v}{r'\omega_p}(1 + \vartheta_1) \tag{15}$$

By combining this equation with the general relations following from the energy balance and the consideration of the centrifugal forces existing in the jet, w_a' and w_t' can be computed; it is

$$w_a' = w_1\left[1 - k\frac{v_1^2}{v_1^2 + (r'\omega_p)^2}\right], \quad w_t' = w_1 k \frac{v_1(r'\omega_p)}{v_1^2 + (r'\omega_p)^2}$$

with

$$k = \frac{\sqrt{1 + \lambda_1^2} - \sqrt{1 + \lambda'^2}}{\vartheta_1 \lambda'}\,\frac{\sqrt{1 + \lambda_1^2}}{\lambda_1} \tag{16}$$

if, for the sake of abreviation, we put:

$$\lambda' = \frac{R}{R'}\lambda = \frac{v}{R'\,\omega_p}, \quad \lambda_1 = (1 + \vartheta_1)\,\lambda' = \frac{v_i}{R'\,\omega_p} \tag{17}$$

(fig. 4). Then the momentum equation gives the thrust loading and the induced efficiency as:

$$c_s = \left(\frac{R'}{R}\right)^2 (i_1 + i_2 - i_3) \tag{18}$$

and

$$\eta_i = \frac{1}{1 + \vartheta_1}\left[1 + \frac{i_2 + i_3}{i_1 - 2\,i_3}\right] \tag{19}$$

whereby*

$$\left.\begin{aligned}
i_1 &= \frac{1}{\frac{\rho}{2}\,R'^2\,\pi\,v^2}\int_0^{R'} \rho\,r'\,\omega_p\,w_t'\,2\,r'\,\pi\,d\,r' \\
&= 2\,k\,\vartheta_1(1 + \vartheta_1)\left[1 - \lambda_1^2\,\ln\left(1 + \frac{1}{\lambda_1^2}\right)\right] \\
i_2 &= \frac{1}{\frac{\rho}{2}\,R'^2\,\pi\,v^2}\int_0^{R'} \frac{\rho}{2}\,w_a'^2\,2\,r'\,\pi\,d\,r' \\
&= \vartheta_1^2\left[1 - 2k\,\lambda_1^2\,\ln\left(1 + \frac{1}{\lambda_1^2}\right) + k^2\frac{\lambda_1^2}{1 + \lambda_1^2}\right] \\
i_3 &= \frac{1}{\frac{\rho}{2}\,R'^2\,\pi\,v^2}\int_0^{R'} \frac{\rho}{2}\,w_t'^2\,2\,r'\pi\,d\,r' \\
&= k^2\,\vartheta_1^2\left[\lambda_1^2\,\ln\left(1 + \frac{1}{\lambda_1^2}\right) - \frac{\lambda_1^2}{1 + \lambda_1^2}\right]
\end{aligned}\right\} \tag{20}$$

*Two typographical errors appearing in Betz-Helmbold's report (reference 2) have been corrected.

This affords a presentation of the (c_s, η_i) curves relating to the different λ by means of the parameter δ_1, provided that the ratio of contraction $\frac{R'}{R}$ is known. It is computed by means of the so-called "contraction equation"

$$\frac{1}{\kappa_1} - \frac{\kappa_2}{\kappa_1} \frac{w_t'}{r' \omega_p} = C \left(1 - \frac{w_t'}{r' \omega_p}\right) \tag{21}$$

where C is the previously cited, assumedly constant quantity, and κ_1 denotes the ratio $\frac{d F'}{d F}$ of the cross section perpendicular to the propeller axis of an individual stream tube in the developed jet to the corresponding section at the propeller circle, and κ_2 the ratio $\frac{F'}{F}$ of a finite disk area $F' = r'^2 \pi$ in the developed jet to the corresponding $F = r^2 \pi$ on the propeller circle and so form the relation

$$\kappa_2 = r'^2 \pi \Big/ \int_0^{r'} \frac{2 r' \pi}{\kappa_1} dr' \quad \text{or} \quad \kappa_1 = \kappa_2 \Big/ \left(1 - \frac{r'}{2 \kappa_2} \frac{\partial \kappa_2}{\partial r'}\right) \tag{22}$$

from equations (21) and (22), κ_1 and κ_2 can be ascertained as functions of r' with the parameter C. The quantity C is finally obtained when κ_1 and κ_2 are introduced in equation

$$\int_0^{R'} \left(2 r' \omega_p w_t' \frac{1}{\kappa_1} - w_t'^2 \frac{\kappa_2}{\kappa_1}\right) 2 r' \pi d r'$$

$$= \int_0^{R'} (2 r' \omega_p w_t' + w_a'^2 - w_t'^2) 2 r' \pi d r' \tag{23}$$

which is obtained when the total propeller thrust is once expressed by the momentum equation through the velocities in the jet and once by means of the Kutta-Joukowsky theorem through the velocities at the propeller circle itself. Having computed C therefrom, the κ_2 taken for this C and $r' = R'$ is the desired contraction ratio. The result is a generally sufficient approximation

$$\left(\frac{R}{R'}\right)^2 = C - (C - 1)\, k\, \frac{\vartheta_1}{1 + \vartheta_1}\, \lambda_1^2 \ln\left(1 + \frac{1}{\lambda_1^2}\right) \tag{24}$$

with $\quad C = 1 + \dfrac{i_2}{i_1 - 2 i_3}$

4. COMPARISON OF THE RESULTS OF BOTH METHODS

Of the two methods for computing the induced efficiency of heavily loaded propellers, the approximation process of section 2 is by far the simpler. Besides the obtained formulas admit of a plausible application to the case of finite blade number (reference 3). It is therefore significant to state that the results achieved by this method are in surprisingly good agreement with the data obtained by the Betz-Helmbold theory. At first it will be shown that both solutions in the vicinity of three limiting cases are in agreement:

a) Light loading (ϑ 0 and ϑ_1 0, respectively, (reference 2, p. 8)): The development of η_i and c_s in equation (7) or (11) for any fixed λ according to the powers of ϑ, gives:

$$\eta_i = 1 - \frac{\vartheta}{2} + \ldots, \quad c_s = 2\vartheta \left[1 - \lambda^2 \ln\left(1 + \frac{1}{\lambda^2}\right)\right] + \ldots$$

Likewise, the expansion of equation (18) to (20) with fixed λ_1 in powers of ϑ_1, gives

$$\eta_i = 1 - \frac{\vartheta_1}{2} + \ldots, \quad c_s = \left(\frac{R'}{R}\right)^2 \left\{2\vartheta_1 \left[1 - \lambda_1^2 \ln\left(1 + \frac{1}{\lambda_1^2}\right)\right] + \ldots\right\}$$

if the relation $k = 1 + \vartheta_1(\ldots) + \ldots$ following from equation (16) is taken into consideration. For $\vartheta_1 \longrightarrow 0$, $w_t' \longrightarrow 0$; then the contraction equation (21) gives $\dfrac{1}{\kappa_1} = \dfrac{1}{\kappa_2} = C$ and hence $\dfrac{R'}{R} = 1$. Accordingly, the (physically plain) relation $\dfrac{R'}{R} \sim 1$ for lightly loaded propellers gives

$$c_s \sim 2\,\vartheta_1 \left[1 - \lambda^2 \ln\left(1 + \frac{1}{\lambda^2}\right)\right]$$

Thus, both solutions give in first approximation

$$c_s \sim 4\,(1 - \eta_i) \left[1 - \lambda^2 \ln\left(1 + \frac{1}{\lambda^2}\right)\right]$$

b) Small coefficient of advance ($\lambda \to 0$, (reference 2, p. 15)): In this case equations (7) and (11) give for fixed ϑ:

$$\eta_i = \frac{1}{1 + \frac{\vartheta}{2}}, \quad c_s \longrightarrow 2\,\vartheta + \vartheta^2 \quad \text{for } \lambda \longrightarrow 0$$

The Betz-Helmbold solution for fixed ϑ_1 gives for $\lambda_1 \to 0$ according to equation (16):

$$k \longrightarrow \frac{1 + \vartheta_1/2}{1 + \vartheta_1}$$

and according to equations (18) to (20):

$$\eta_i \longrightarrow \frac{1}{1 + \frac{\vartheta_1}{2}}, \quad c_s \longrightarrow \left(\frac{R'}{R}\right)^2 \left(2\,\vartheta_1 + 2\,\vartheta_1^2\right)$$

For vanishing efficiency $\frac{w_t'}{r'\,\omega_p} \longrightarrow 0$; for it equation (21) gives

$$\frac{1}{\kappa_1} = \frac{1}{\kappa_2} = C \quad \text{and hence} \quad \left(\frac{R'}{R}\right)^2 = \frac{1 + \vartheta_1/2}{1 + \vartheta_1}$$

Accordingly the application of

$$\left(\frac{R'}{R}\right)^2 \sim \frac{1 + \vartheta_1/2}{1 + \vartheta_1}$$

to small coefficient advance gives

$$c_s \sim 2\,\vartheta_1 + \vartheta_1^2$$

Hence both solutions give for $\lambda \longrightarrow 0$ in first approximation

$$c_s \sim \frac{4(1 - \eta_i)}{\eta_i^2}$$

c) Great coefficient of advance ($\lambda \longrightarrow \infty$): To show the accord of both solutions at high coefficients of advance, we first develop equation (12) for fixed ϑ according to the powers of $\frac{1}{\lambda}$ and obtain - terms of higher than second order being disregarded in $\frac{1}{\lambda}$ -

$$c_s \sim \frac{2(1 - \eta_i)}{\eta_i} \left(\frac{\eta_i}{\lambda}\right)^2 \tag{25}$$

The corresponding expansion of the Betz-Helmbold quantities for fixed ϑ_1 in powers of $\frac{1}{\lambda_1}$ gives according to equation (16):

$$k = \frac{1 + \vartheta_1}{\vartheta_1} \frac{1 + \lambda_1^2}{\lambda_1^2} - \frac{1}{\vartheta_1} \sqrt{1 + \frac{1}{\lambda_1^2}} \sqrt{1 + \left(\frac{1 + \vartheta_1}{\lambda_1}\right)^2}$$

$$= 1 - \frac{\vartheta_1}{2} \frac{1}{\lambda_1^2} + \ldots\ldots$$

which, written in equation (18) to (20) for c_s and η_i, gives:

$$\eta_i = \frac{1 + \frac{\vartheta_1}{2}}{1 + \vartheta_1} + (\ldots) \frac{1}{\lambda_1^2} + \ldots$$

$$c_s = \left(\frac{R'}{R}\right)^2 \left[\vartheta_1 \left(1 + \frac{\vartheta_1}{2}\right) \frac{1}{\lambda_1^2} + \ldots\right] \tag{26}$$

For $\lambda_1 \longrightarrow \infty$, $\dfrac{w_{t'}}{r' \omega_p} \longrightarrow \dfrac{\vartheta_1}{1 + \vartheta_1}$; and equation (21) yields:

$\kappa_1 = \kappa_2 = \dfrac{1 + \vartheta_1}{C + \vartheta_1}$, hence $C = 1$ and $\dfrac{R'}{R} = 1$. Accordingly, the use of the (physically plausible) relation $\frac{R'}{R} \sim 1$ for high coefficients of advance yields

$$c_s \sim \vartheta_1 \left(1 + \frac{\vartheta_1}{2}\right) \frac{I}{\lambda^2} \tag{27}$$

From equations (26) and (27) therefore follows:

$$c_s \sim \frac{2(1 - \eta_i)}{\eta_i} \left(\frac{\eta_i}{\lambda}\right)^2$$

in accordance with equation (25).

In order to obtain a further basis for the order of agreement of both solutions, various (c_s, η_i) curves were computed by both methods. For instance, the values of λ, η_i, and c_s were computed for $\lambda' = \dfrac{R}{R'} \lambda = 1$ and a series of ϑ_1 values by the Betz-Helmbold method with equations (17) to (20) and (24). The results are indicated as solid curve marked $\lambda' = 1$ in figure 5. Then the corresponding value c_s for each thus computed pair of λ, η_i was computed according to the approximation (equation (12)) for comparison. The result, the dotted curve $\lambda' = 1$, is shown in figure 5. The same calculation was repeated for $\lambda' = 0.5$ and $\lambda' = 2$. In both cases the (c_s, η_i) curve obtained by Prandtl's approximation (dashed curve, fig. 5) manifests a surprisingly good agreement with the (c_s, η_i) curve (solid curve, fig. 5) computed according to the Betz-Helmbold method.

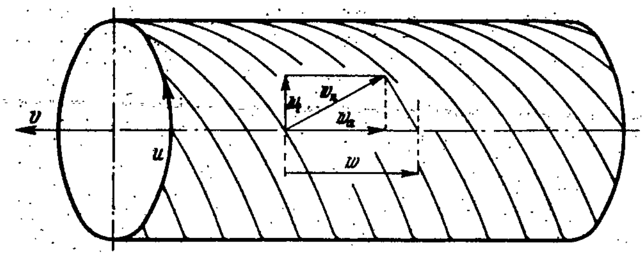

Figure 1.

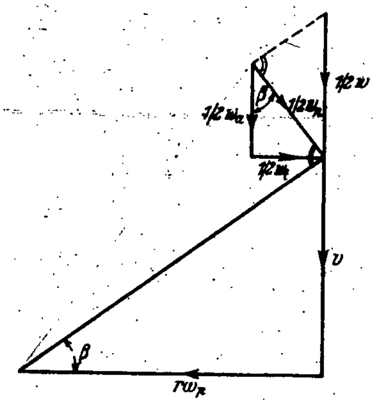

Figure 2.

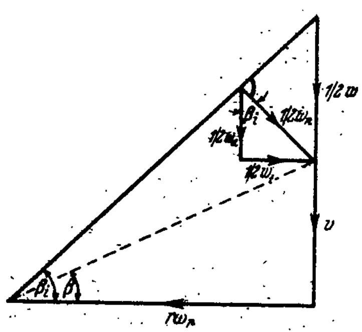

Figure 3.

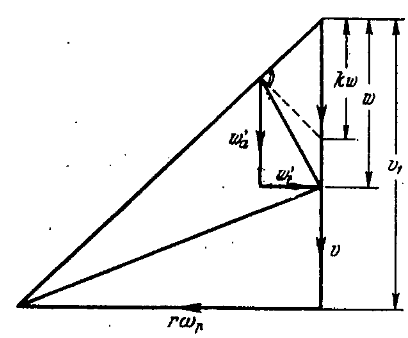

Figure 4.

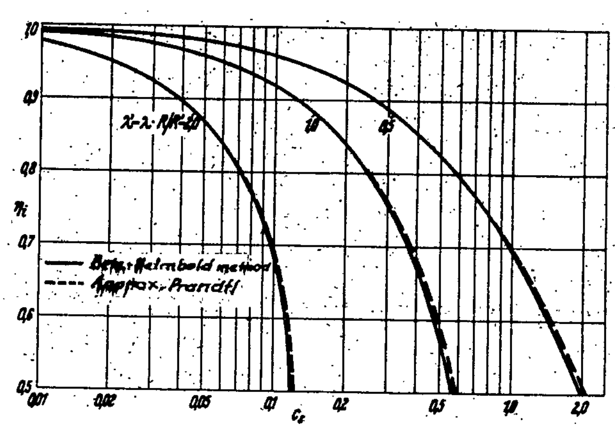

Figure 5.

REFERENCES

1. Betz, A.: Schraubenpropeller mit geringstem Energieverlust. Mit einem Zusatz by L. Prandtl. Nachr. der K. Gesellschaft der Wissenschaften zu Göttingen, Math.-phys. Kl. (1919), pp. 193-217. Abgedruckt in L. Prandtl und A. Betz, Vier Abhandlungen zur Hydrodynamik und Aerodynamik, Göttengen (1927), pp. 68-92.

2. Betz, A., and Helmbold, H. B.: Zur Theorie stark belasteter Schraubenpropeller. Ingenieur-Archiv, Bd. 3 (1932), pp. 1-23.

3. Kramer, K. N.: Induzierte Wirkungsgrade von Best-Luftschrauben endlicher Blattzahl. Luft-Forsch. Bd. 15 (1938) Lfg. 7, pp. 326-333. (See p. 18 of this Technical Memorandum.)

LEGENDS

w, impact velocity

w_n, interference velocity

w_a, axial interference velocity

w_t, tangential interference velocity

Figure 1.- Traces of the propeller.

Figure 2.- Components of interference velocity on blade element at distance r from the axis.

Figure 3.- Induced angle of advance β_i.

Figure 5.- Induced efficiency of optimum propellers by Betz-Helmbold versus Prandtl method.

THE INDUCED EFFICIENCY OF OPTIMUM PROPELLERS HAVING A FINITE NUMBER OF BLADES*

By K. N. Kramer

SUMMARY

The load coefficients c_s and c_l related to an induced efficiency η_i are in part determined by exact calculation and in part by interpolation for 2, 3, 4, 6, and 8 blades and any coefficient of advance λ. The results are presented in two charts, figures 8 and 9.

1. INTRODUCTION

The highest possible induced efficiency η_i for free-running propellers can be computed from the assumption of optimum circulation distribution and vanishing profile drag as the ratio of effective to input power : S v : N. Its importance in the evaluation of the quality of constructed propellers as in general considerations about the energy balance of an airplane is similar to that of the induced drag of a wing with elliptic lift distribution. Now, the majority of formulas used in practice are based on the assumption of light loading and infinite blade number or else involve a subsequent conversion to finite blade number by correction factors based on the premise of small coefficient of advance and requiring a discussion of its range of application. But, as airplane speeds increase, i.e., as the coefficients of advance increase, the thrust reduction toward the slipstream boundary due to the finite blade number becomes more and more effective and so makes it increasingly necessary to take the actual number of blades into consideration.

Aside from that, the more rapid drop in efficiency calls for formulas which promise adequate correctness down to $\eta_i = 0.50$.

---

*"Induzierte Wirkungsgrade von Best-Luftschrauben endlicher Blattzahl." Luftfahrtforschung, vol. 15, no. 7, July 6, 1938, pp. 326-333.

The reason that these improvements have not been carried out simultaneously until now, is partly due to the fact that, while the solution of the optimum circulation distribution rests, according to Betz (reference 1), on a simple physical statement, the evaluation in conformity with the solution of Goldstein's potential problem (reference 2) for finite blade number becomes more troublesome and wearisome as the coefficient of advance becomes greater. Furthermore, the so-computed distribution is, strictly speaking, optimum only for light blade loading, while for the thrust and performance coefficients of heavily loaded propellers, there exists only Prandtl's approximation (reference 1), and for the infinite-blade propeller only the Betz-Helmbold theory (reference 3), which is directly applicable to finite blade number. The basic principles of the last two have been described in the preceding report by F. Lösch.

In view of the marked agreement of these results down to $\eta_i = 0.50$, the same process is to be followed for finite blade number. The thrust formula (reference 4, equations (11) and (8)) is suitably transformed for finite blade number

$$c_s = \frac{8(1 - \eta_i)}{\eta_i} K_{31}^{(z)} + \frac{8(1 - \eta_i)^2}{\eta_i^2} K_{52}^{(z)} \qquad (1.1)$$

and with it the formula for the power loading:

$$c_l = \frac{c_s}{\eta_i} = \frac{8(1 - \eta_i)}{\eta_i^2} K_{31}^{(z)} + \frac{8(1 - \eta_i)^2}{\eta_i^3} K_{52}^{(z)} \qquad (1.2)$$

Hereby the optimum circulation distribution

$$\underline{G}^{(z)} = \kappa\ \underline{G}^{(\infty)} = \kappa \frac{x^2}{\lambda_i^2 + x^2} \qquad (1.3)$$

replaces $\underline{G}^{(\infty)}$ and

$$K_{m,n}^{(z)} = \int_0^1 \frac{\kappa\ x^m}{(\lambda_i^2 + x^2)^n} d\,x \qquad (1.4)$$

replaces $K_{m,n}^{(\infty)}$. The factor κ is as in Helmbold's report (reference 5) called "average factor." It gives the effect of the blade number z and depends, like $\underline{G}^{(z)}$ on the location $x = r : R$ of the propeller element and on the "induced coefficient of advance:"

$$\lambda_i = \frac{\lambda}{\eta_i} \tag{1.5}$$

For infinite blade number (reference 4, p. 323), the function is $\kappa = 1$ and the integrals $K_{m,n}^{(\infty)}$ are integrable. For instance, it is:

$$K_{31}^{(\infty)} = \frac{1}{2}\left[1 - \lambda_i^2 \ln\left(1 + \frac{1}{\lambda_i^2}\right)\right] \tag{1.6}$$

$$K_{52}^{(\infty)} = \frac{1}{2}\left[1 + \frac{1}{1 + \frac{1}{\lambda_i^2}} - 2\lambda_i^2 \ln\left(1 + \frac{1}{\lambda_i^2}\right)\right] \tag{1.7}$$

According to Goldstein (reference 2), $\underline{G}^{(z)}$ should be computed for finite blade number for each z and λ_i, and κ computed therefrom according to equation (1.3), and then $K_{31}^{(z)}$ and $K_{52}^{(z)}$ defined by planimetry.

In the following, the already available calculations for the two-blade propeller are first extended to cover any great coefficient of advance (section 2). Then it is attempted to forego the rest of the calculation for other blade numbers and to ascertain the integral values direct by interpolation (section 3). In conjunction with a further method of interpolation, it succeeds in presenting the entire results in a practical chart (section 4), which gives, aside from the unavoidable efficiency drop due to the axial energy of the slipstream (axial efficiency η_a of elementary jet theory), the induced propeller efficiency for 2, 3, 4, 6, 8, and ∞ number of blades (section 5). Then the gain in efficiency due to increased blade number is immediately apparent. One particular advantage accruing therefrom is that the effect of the profile lift/drag ratio ϵ_p (assumed constant over the blade) on the efficiency is approximately independent from the number of blades, as will be proved in a later report.

2. CALCULATIONS FOR THE TWO-BLADE PROPELLER

The starting point and at the same time the major part of the whole task lies in the solution of the optimum circulation distribution $\underline{G}^{(z)}(x;\ \lambda_i)$. As this involves the use of series of Bessel functions, which for the most are available in tables for even but not uneven z, the majority of evaluations had been made only for the two-blade propeller rather than the much more common three-blade propeller. Such distributions were available*

a) for $\lambda_i = \frac{1}{10};\ \frac{1}{9};\ldots\ldots;\frac{1}{3};\ \frac{1}{2}$ (Goldstein (reference 2, p. 450));

b) for $\lambda_i = \frac{1}{5};\ \frac{1}{4};\ \frac{1}{3};\ \frac{2}{5};\ \frac{1}{2};\ \frac{2}{3}$ (Lock-Yeatman (reference 6, p. 25, table 7)).

The latter - based in part on Goldstein's interim results - are the result of a series transformation improving the convergence and for that reason are slightly different from Goldstein's figures especially in proximity of the blade tip. But at the very tip (x = 1), Goldstein as well as Lock would have found $\underline{G} = -0.024;\ -0.046;\ -0.059$ for $\lambda_i = \frac{1}{5};\ \frac{1}{3};\ \frac{1}{2}$ as is readily proved, whereas a simple physical consideration calls for value zero, just as the circulation disappears at the edge of a wing of finite span. Hence the error, which in the tables cited under a) and b) amounts at the blade tip to 3; $8\frac{1}{2}$; 17 percent of the maximum circulation, rests on the inaccuracy of the constants involved in the series of Bessel functions, computed by Goldstein as variables in a system of infinitely many

*These tables contain the optimum distribution $\underline{G}$, respectively indicated by $\Gamma\,\omega/\pi\ w\ v$, or $\kappa \cos^2 \Phi$ for agreeing arguments $x : \lambda_i$, indicated with μ and $\cot\ \Phi$, respectively.

linear equations. No doubt the error decreases from the blade tip inward, but its rate of decrease is not summarily predictable, neither is the effect on $K^{(2)}_{31}$ and $K^{(2)}_{52}$ at which the outer blade zones enter more heavily than the inner zones, nor the extent of impairment of the interpolation in reference 6, p. 17, table 1.

Either Lock's or Goldstein's calculating method would have entailed too much paper work for coefficients of advance of 1 or more. Further series transformations together with a suitable premise for the solutions of the equation systems involved made it possible to carry out the calculation of $\underline{G}$ for any other high coefficient of advance and any number of blades with greater accuracy and in less time. Neither the derivation nor the calculating procedure can be discussed here. But the results of the evaluations made so far shall be published.

Table I gives the optimum circulation distributions for the 2-blade propeller, while figure 6 shows various related optimum distributions of the infinite-blade propeller for comparison. The correlated infinite equation systems for $\lambda_i = \frac{1}{4}$ and $\frac{1}{3}$ were solved anew, the values in the table cited under b) corrected accordingly and the intermediate points obtained by accurate plotting. In addition, all calculations for all arguments were carried through for $\lambda_i = \frac{1}{2}$, 1, and 2.5. A remarkable confirmation was found for the values of $\lambda_i = 2.5$ through the approximation for great coefficients of advance following from the expansion of $\underline{G}^{(2)}$ in powers of $\frac{1}{\lambda}$:

$$\underline{G}^{(2)} \approx \frac{x\sqrt{1-x^2}}{\pi}\left[\frac{1}{\lambda_i^{\,2}} - \frac{2\,x^2+1}{6}\,\frac{1}{\lambda_i^{\,4}}\right] \qquad (2.1)$$

The discrepancies over the whole radius were less than 1 percent for $\lambda_i = 2.5$. The first term of the expansion coincided with the solution - known through conformal transformation - of the potential problem of rotating strip for infinite coefficient of advance.

TABLE I - Optimum Circulation Distribution $\left(\frac{G}{\pi}\right)^{(a)}$

for the 2-Blade Propeller

x	$\lambda_i = \frac{1}{4}$	$\lambda_i = \frac{1}{3}$	$\lambda_i = \frac{1}{2}$	$\lambda_i = 1.0$	$\lambda_i = 2.5$
0.1	0.232	0.164	0.0919	0.0283	0.00494
.2	.418	.303	.1758	.0552	.00974
.3	.548	.412	.246	.0795	.01415
.4	.629	.486	.297	.0999	.01806
.45	.655	.510	-	.1082	.01976
.5	.671	.528	.331	.1155	.02124
.6	.679	.540	.345	.1239	.02342
.7	.654	.517	.338	.1243	.02423
.75	.623	.493	.325	.1213	.02396
.80	.580	.457	.305	.1156	.02310
.85	.528	.413	.276	.1061	.02147
.90	.449	.351	.235	.0919	.0187
.925	.395	.311	-	.0817	.0168
.95	.329	.260	.173	.0687	.0141
.975	-	.19	-	.0497	.0103
$\underline{G}_{max}$ =	.679	.540	.345	.125	.0242

Table II gives the average factor κ defined by equation (1.3). It indicates the ratio of optimum circulation for $z = 2$ to that for $z = \infty$ for equal coefficient of advance and efficiency on corresponding blade radii, or more explicitly: the ratio of average axial interference velocity w_a (in time rate) behind a 2-blade propeller to the (constant in time) interference velocity at the same point behind a propeller of infinite number of blades. For high coefficients of advance, equation (2.1) affords the approximation

$$\kappa \approx \frac{\sqrt{1 - x^2}}{\pi \, x} \left[1 + \frac{4 \, x^2 - 1}{6} \, \frac{1}{\lambda_i^{\,2}} \right] \tag{2.2}$$

TABLE II - Average Factor $\kappa = \underline{G}^{(2)} : \underline{G}^{(\infty)}$

for the 2-Blade Propeller

$\lambda_i = \frac{\tan \phi}{r/R}$

x \ λ_i =	1/4	1/3	1/2	2/3	1.0	2.5	∞
0.1	1.682	1.987	2.390	2.62	2.858	3.092	3.167
.2	1.071	1.146	1.274	1.35	1.436	1.532	1.559
.3	929 .929	.920	927 .927	.940	.963	.997	1.012
.4	.874	.823	.760	.733	.724	.724	.729
.45	.857	.790	-	.668	655 .643	.630	.632
.5	.839	.762	.663	.612	.577	.552	.551
.6	.797 .797	.706	.590 .585	.522	.468	.430	.424
.7	.737	.635	.510	.442	.378	.333	.325
.75	.692	.591	.469	.399	.350 .337	.290	.281
.8	.637	.537	.424	.356	.296	.249	.239
.85	.574	.477	.372	.310	.253	.207	197 .197
.9	.484	.399	.307	.252	.208 .205	.163	.154
.925	.424	.351	-	.22	.177	.139	.131
.95	.352	.292	.220	.182	152 .145	.112	105 .105
.975	-	.21	-	.13	.102	.078	.073

The first term supplied in figure 7 the boundary points of the parameter curves on the ordinate axis $(1 : \lambda_i = 0)$, the second term the curvature parabolas at those points. This diagram allows an exact interpolation of $\underline{G}^{(2)}$ to a prescribed λ_i: read the ordinates above the relative abscissa for the different parameters x and compute $\underline{G}$ in equation (1.3). Thus, it is seen that the distribution for $\lambda_i = \frac{2}{3}$ cited under b) is much more accurate than that for $\lambda_i = \frac{1}{2}$ and requires only minor changes for the extreme blade points.

The two columns for $K_{31}^{(2)}$ and $K_{52}^{(2)}$ in table III are the result of planimetration. The following are practical approximate formulas for all coefficients of advance:

$$K_{31}^{(2)} \approx \frac{1}{2 + 2.5\ \lambda_i + 16\ \lambda_i^{\,2}} \tag{2.3}$$

and

$$K_{52}^{(2)} \approx \frac{1}{2 + 2\ \lambda_i + 32\ \lambda_i^2 + 32\ \lambda_i^{\,4}} \tag{2.4}$$

The premise for these so posed that they give, on the one hand, the correct values 1/2 for $\lambda_i = 0$ and, on the other, agree for $\lambda_i \longrightarrow \infty$ in the first terms of the series expansions with those following from equation (2.2). Through choice of the middle terms in the denominators, equation (2.3) gave as maximum relative error +3 percent at $\lambda_i \approx \frac{1}{3}$ and -3 percent at $\lambda_i \approx 3$, while the values in equation (2.4) are 5 percent too low at $\lambda_i \approx \frac{1}{2}$. As first application the integral values for $\lambda_i = 1.5$ and 2.0 were interpolated by plotting the differences between the exact values of the table and the approximations from the above formulas.

$$\gamma_{31}^{(z)} = \frac{K_{31}^{(z)}}{K_{31}^{(\infty)}} \quad \text{or} \quad \gamma_{52}^{(z)} = \frac{K_{52}^{(z)}}{K_{52}^{(\infty)}} \tag{2.5}$$

TABLE III - Integral Values and Equivalence Factors

for the 2-Blade Propeller

λ_i =	$K_{31}^{(2)}$ =	$K_{52}^{(2)}$ =	$\gamma_{31}^{(2)} = \frac{K_{31}^{(2)}}{K_{31}^{(\infty)}}$	$\gamma_{52}^{(2)} = \frac{K_{52}^{(2)}}{K_{52}^{(\infty)}}$
0	0.5	0.5	1	1
1/10	.410	.392	0.860	0.854
1/9	.398	.378	.842	0.837
1/8	.385	.362	.824	0.819
1/7	.368	.341	.800	0.792
1/6	.345	.312	.766	0.755
1/5	.313	.274	.720	.704
1/4	.270	.222	.656	.631
1/3	.211	.156	.567	.532
1/2	.1353	.0807	.453	.408
2/3	.0919	.0436	.386	.335
1.0	.0493	.0151	.321	.266
1.5	.0245	.0043	.283	.226
2.0	.0144	.00156	.269	.210
2.5	.00952	.000689	.263	.202
great	eq. (2.7)	eq. (2.8)	eq. (2.9)	eq. (2.10)
∞	0	0	0.25	.1875

Table III also contains the "equivalence factors" for $z = 2$, i.e., the ratio of the planimetric integral values for the 2-blade propeller to the integral computed from equation (1.6) or (1.7) of the modified jet theory by the same argument λ_i. An infinite-blade propeller with fixed λ relative to induced efficiency η_i is "equivalent" to a 2-blade propeller (of identical swept-disk area) whose thrust and performance coefficients are smaller in a ratio which, according to equation (1.1) or (1.2) by small loading $(\eta_i \simeq 1)$ is equal to $\gamma_{31}^{(2)}$ and with increasing load $(\eta_i \longrightarrow 0.50)$ shifts toward $\gamma_{52}^{(2)}$. But to read therefrom, equivalence respecting thrust and power for different swept-disk areas is not absolutely expedient, since either the engine r.p.m. or the coefficient of advance of the blade tip must change with the diameter.

At last the curves of constant induced efficiencies can be computed. Starting with a sequence of values λ_i for which the integral values are read from table III, the values computed according to equation (1.1) or (1.2), respectively, then belong to the coefficients of advance $\lambda = \eta_i \lambda_i$ and later give the parameter curve η_i = const. in a double logarithmic (λ, c_s) or (λ, c_l) chart, respectively. Note the axis of abscissa, $z = 2$, in figures 13 and 14 to which the plotted chart corresponds.

For $\lambda = 0$, but $\eta_i \neq 0$ would be $\lambda_i = 0$, hence $\kappa = 1$; $K_{31} = K_{52} = 1/2$ and

$$c_s = \frac{4(1 - \eta_i)}{\eta_i^2}$$

Hence, the parameter curves approach in the logarithmic chart left-hand horizontal asymptotes.

Actually, however, $\eta_i = 0$ at static thrust; $\lambda_i = \lim \frac{\lambda}{\eta_i} \neq 0$ and c_s becomes infinite, so that these asymptote values have no significance for the evaluation of the static thrust itself. But they do prove useful in an appraisal of the conditions at nonvanishing coefficient of advance, because the just-cited equation rests on the premise of vanishing twist and uniform axial velocity distribution across the jet section. It is identical with the well-known formula for the axial efficiency

$$\eta_a = \frac{2}{1 + \sqrt{1 + c_s}} \tag{2.6}$$

and gives the efficiency decrease unavoidable for producing a certain thrust. Accordingly, reading the efficiency for a certain c_s (or c_l) in figure 13 (or fig. 14) on the left-hand horizontal asymptotes, it corresponds to the simple jet theory. But a more exact theoretical upper limit for the free-running 2-blade propeller would be a smaller efficiency to be read with the same ordinate over the pertinent efficiency. The difference of both indicates the highest possible gain obtainable by the most ideal guide apparatus behind such a one without enlarging the jet section and by equal postulated total thrust (or equal power input of propellers).

As the coefficient of advance increases, the slipstream twist as well as its nonuniformity, because of the finite blade number, effects an always greater decrease in efficiency. A thrust formula for $z = 2$ could be evolved from equations (2.3) and (2.4) suitable for all coefficients of advance, but which would be quite cumbersome and become of the 6th order in η_i.

On the other hand, equation (2.2) affords the following simple beginnings of series expansions which are suitable as approximations for great λ_i:

$$K_{31}^{(2)} = \frac{1}{16\,\lambda_i^{2}} - \frac{1}{48\,\lambda_i^{4}} + \ldots\ldots \tag{2.7}$$

$$K_{52}^{(2)} = \frac{1}{32\,\lambda_i^{4}} - \frac{1}{32\,\lambda_i^{6}} + \ldots\ldots \tag{2.8}$$

$$\gamma_{31}^{(2)} = \frac{1}{4} + \frac{1}{12\,\lambda_i^{2}} + \ldots\ldots \tag{2.9}$$

$$\gamma_{52}^{(2)} = \frac{3}{16} + \frac{3}{32\,\lambda_i^{2}} + \ldots\ldots \tag{2.10}$$

$$c_s = \frac{(1 - \eta_i)\,\eta_i}{2\,\lambda^2}\left[1 - \frac{\eta_i(5\,\eta_i - 3)}{6\,\lambda^2} + \ldots\right] \tag{2.11}$$

$$c_l = \frac{1 - \eta_i}{2\lambda^2}\left[1 - \frac{\eta_i(5\,\eta_i - 3)}{6\,\lambda^2} + \ldots\right] \tag{2.12}$$

The equations obtained by omitting the points are practical to coefficients of advance as low as 1.5. At λ_i = 1.5, $K_{31}^{(2)}$ is obtained from equation (2.7) only 4 percent too low, while the error of c_s in equation (2.11) is even less than that.

In first approximation, the factors before the brackets should be used. Then the curves of constant efficiency approach toward the right, straight lines with the pitch -2. η_i is ambiguous function of c_s; the maximum values

$$c_{s\ max} = \frac{1}{8\,\lambda^2} \tag{2.13}$$

give $\eta_i = 0.50$.

Only the efficiences above 50 percent are of practical significance:

$$\eta_i{}^* = \frac{1}{2} + \frac{1}{2}\sqrt{1 - 8\,\lambda^2\ c_s} \tag{2.14}$$

the * sign serving as reminder that the equation is correct only for great coefficients of advance.

3. FIRST METHOD OF INTERPOLATION TO ANY BLADE NUMBER

Proceeding from the exact calculations for $z = 2$ and $z = \infty$, the integral values can be accurately interpolated without determination of the circulation distributions for arbitrary blade number, by combining two ideas, one of which affords information for very small, the other for infinite coefficient of advance. Optimum circulations were already available for $z = 3$ and $z = 4$, some earlier computed by the DVL, some tabulated by Lock-Yeatman (reference 6, p. 26). Since both calculations proceeded from simplifying assumptions apt to produce increasing errors as the coefficient of advance increases, the discrepancies in these tables are considerable. They are therefore used only up to medium coefficients of advance as base for the more exact shape of the curves to be described. For the less important numbers of blades, 6 and 8, (reference 1) the slightly less accurate method is used.

For small coefficients of advance, the boundaries of the propeller vortex surfaces follow in very close sequence. The distance of two adjacent boundary curves (more exact: the vertical distance of the two parallel straight lines obtained by development in the plane) is:

$$a = \frac{2}{z} \frac{\lambda_i}{\sqrt{1 + \lambda_i^2}} \pi R$$

and becomes small in relation to the diameter for great blade number or small λ_i. This makes the flow for median blade zones comparable with that for infinite blade number, and the potential flow about the edges of the propeller vortex surfaces with a screen flow on parallel half-planes at distance a. L. Prandtl (who originally made these comparisons (reference 1)) obtained his well-known approximate formula for κ, and hence for $\underline{G}$, with them. We do not use Prandtl's equation itself, but the statement that at small coefficients of advance equal κ distributions and consequently approximately equal value of $\gamma_{m,n}^{(z)}$ belong to different arguments for z and λ_i, for which only

$$\frac{a}{\pi R} = \frac{2}{z} \frac{\lambda_i}{\sqrt{1 + \lambda_i^2}} \tag{3.1}$$

assumes the same value. It is Helmbold's suggestion (reference 5, fig. 3) to plot instead of λ_i the value of the expression (3.1) on the abscissa, starting at the origin. Using it as in figures 8 and 9, the values of λ_i and the abscissa for any blade number can be obtained without calculation. Another advantage for the interpolation is the finite abscissa length for the infinite range of λ_i.

Plotting the equivalence figures $\gamma_{31}^{(2)}$ and $\gamma_{52}^{(2)}$ for the 2-blade propeller of table III in figures 8 and 9 affords a pair of monotonic curves, which closely hug the tangent in the right-hand end point prescribed by equations (2.9) and (2.10), respectively. According to Prandtl's concept, the corresponding curves for other blade numbers starting at the left top corner must for a short distance follow very closely to the plotted curve.

For infinite coefficient of advance, Westwater (reference 7) has derived an infinite series for κ as generalization of the first term in equation (2.2) to any blade number by conformal transformation, which he evaluated for $z = 3$ and $z = 4$. As generalization of the coefficients of the first terms in equations (2.7) and (2.8), a term-by-term integration in Westwater's series affords an even more simple series of the values

$\left(\lambda_i^{2n} K_{m,n}\right)^* = \left(\lambda_i^{2n} K_{m,n}\right)$ for $\lambda_i = \infty$, which, for $z = 1$ and $z = 2$, can be interrupted after a few terms and remain summable even for $z = 4$.

It gave for	$z = 1$	$z = 2$	$z = 3$	$z = 4$	$z = 6$	$z = 8$	$z = \infty$
$(\lambda_i^2 K_{31})^* =$	9:256	1:16	0.0846	$1:\pi^2$	0.127	0.1455	1:4
$(\lambda_i^4 K_{52})^* =$	35:2048	1:32	.044	$1:6\pi$	.069	.0809	1:6

and hence

$\gamma_{31}^* =$	0.1406	0.2500	0.338	0.4053	0.51	0.582	1
$\gamma_{52}^* =$	.1025	.1875	.264	.3183	.41	.485	1

The related points in figures 8 and 9 are denoted with * and constitute as exact and readily computed end points of the desired curves a substantial aid for the interpolation. A glance, especially at figure 8, reveals that these end points are quite close to the curve $z = 2$ and, since all curves probably vary monotonically as for $z = 2$, it approximately follows that the equivalence figures $\gamma_{31}^{(z)}$ for the customary blade numbers and for all coefficients of advance are related to $\frac{2}{z} \frac{\lambda_i}{\sqrt{1 + \lambda_i^2}}$ only. In other words: The agreement in the sense of Prandtl's theorem still holds at high rises for the equivalence figures γ_{31}, long after the related κ distributions and the values of K_{31} and $\lambda_i^2 K_{31}$ have become markedly unlike. This "fortunate accident," however, does not appear so very remarkable any more if expressed in more simple terms as follows: The percent thrust loss due to flow around the edges of the propeller surfaces is largely dependent upon the ratio of boundary curve distance to jet circumference only.

For the more precise determination of the curves for the 3- and 4-blade propellers in figures 8 and 9, earlier calculations were resorted to. The maximum error for $\lambda_i = 1$ does not exceed 4 percent. By the opposite process, the integral values can be determined with the same accuracy and the thrust and power charts computed for each individual blade number, as effected for the 2-blade propeller.

The ratio of the "equivalent" (small) thrusts or power for the same induced efficiency and coefficient of advance can be directly read from figure 8; for instance, between the 2- and 3-blade propellers, it is $\gamma_{31}^{(2)}:\gamma_{31}^{(3)}$. But in practice the case is usually the opposite: the gain in η_i by increasing the number of blades for a fixed thrust loading c_s (or power loading c_l) is of interest. It is therefore desirable to combine the efficiency curves for all blade numbers into one chart. Unfortunately, not even the approximate law achieved for the equivalence figures γ_{31} is readily transferable. Neither is a transformation of the ordinate c_s (or c_l) possible in relation to the blade number, applicable to all coefficients of advance, nor do corresponding efficiency curves for different blade numbers lend themselves to combination by vertical displacement. On the other hand, the set task can be accomplished by a transformation of the abscissa as shown in the next section.

4. SECOND METHOD OF INTERPOLATION AND DESIGN OF THE CHARTS

Figure 10 shows the most important integral values K_{31} for $z = 2$ and $z = \infty$ blades. With the logarithmic scale employed, the vertical distance of two points over the same abscissa λ_i indicates the equivalence figure $\gamma_{31}^{(z)}$, which so far guided the interpolation. Now, however, the two curves merge with better agreement through horizontal than through vertical displacement, as disclosed by plotted tangents. A similar behavior may be looked for for the intermediate curves $z = 3; 4; \ldots$. The horizontal distance of the points of the curves which presents the ratio of the arguments λ_i with equal function values K_{31}, is therefore, even if physically not quite so logical, a particularly suitable quantity for the interpolation, because of its fluctuation within narrow limits for any number of blades z.

The lengths by which the points of curve $z = 2$ had to be shifted horizontally to the right in a logarithmic abscissa scale of unit 125 mm, until they merged with curve $z = \infty$, have been plotted in figure 11 against the related values λ_i (scale of abscissa again according to equation (3.1) as in figures 8 and 9). The result is the curve marked $z = 2$. The ratio of the correlated coefficients of advance can be read from a further ordinate scale. For the still missing curves, the points for very small coefficients of advance were approximated and the correct end points for $\lambda_i = \infty$ exactly determined. The known curve $z = 2$ must gradually merge with the horizontal course of the axis ($z = \infty$), so that the curves $z = 3, 4, \ldots$, can be plotted fairly accurately. Further improvements can be made by comparison with figure 8 and some refinements, whereby the two interpolation methods supplement one another quite well. It will be found that the presumed law of constant abscissa displacement is even much better fulfilled if the distances are measured from curve $z = 2$ instead of from $z = \infty$.

For the transference of this law to figures 13 and 14, which already contain the curves of constant efficiencies for $z = 2$, it is important that for every constant η_i the ratio of λ_i be equal to the ratio of the geometric λ itself. Moreover, at light loading ($\eta_i \approx 1$), equal values $K_{31}^{(z)}$ according to equations (1.1) and (1.2) have equal thrust and power loading for different blade numbers.

A similar statement is not possible for $k_s = c_s \lambda^2$ or $k_l = c_l \lambda^3$, because factor λ^2 or λ^3 is involved. This explains why figure 14, for instance, gives the power loading c_l rather than the more common power factor k_l. Even so, figure 14 can be used in computations with k_l, since $k_l = c_l \lambda^3 = \text{const.}$ is presented by straight lines of pitch -3. It should be noted, however, that each blade number z has a different straight line as a result of the abscissa transformation.

With increasing loading, the effect of K_{52} may become disturbing: For the curve $\eta_i = 0.50$, on account of

$$c_s = 8\ K_{31}^{(z)} + 8\ K_{52}^{(z)}$$

the abscissa transformation for the function $(K_{31} + K_{52})$ rather than K_{31} is decisive, as shown in figure 12. A helpful fact is that the end points for infinite coefficient of advance are exactly the same as in figure 11, since K_{31} disappears quadratically in $\left(\frac{1}{\lambda_i}\right)$, but K_{52} of the fourth order. The abscissa displacement for large coefficients of advance is thus uniformly determined for all efficiency curves by γ_{31}^*, which, moreover, can be quite accurately expressed by $\frac{z}{z + 6}$. By indicating with "equivalent coefficients of advance" those which for different blade numbers by equal induced efficiency η_i have equal coefficients c_l and c_s, the formula may be expressed as follows:

The squares of equivalent coefficients of advance are, for very large coefficients of advance, exact, and for customary coefficients of advance, approximately like the inverse equivalence figures γ_{31}^*, that is, about like $\left(z + \frac{6}{z}\right)$. At the same time, the formula (2.14), practical for $\lambda > 2$ can be generalized for any blade number as:

$$\eta_i^* = \frac{1}{2} + \frac{1}{2}\sqrt{1 - \left(2 + \frac{12}{z}\right) \lambda^2 c_s} \qquad (4.1)$$

Strictly speaking, the abscissa transformation is somewhat related to the efficiency, as a comparison of figures 11 and 12 shows. But, since we proceed from two blades, the discrepancy is not noticeable for less than 6 and 8, or an infinity of blade numbers, where our interest is solely theoretical and exact figures are available from the modified jet theory. Moreover, while this discrepancy increases with decreasing coefficient of advance, the flattening out of the efficiency curves lessens its importance again. And if, in addition, the displacement is referred to $\eta_i = 0.90$, as effected in figures 13 and 14, the error within the presented range remains within the accuracy of the interpolation methods. The result for the charts (figs. 13 and 14), which are exact for $z = 2$, is that the potential error in efficiency for $z = 3$, and $z = 4$, will scarcely exceed the inaccuracy of reading.

5. USE OF CHARTS

Figures 13 and 14 illustrate the functional relationship between coefficient of advance λ, blade number z, thrust loading c_s (power loading c_l) and the induced efficiency η_i of the free-running optimum propeller.

Given, for instance, λ, z, and c_l, and seeking the induced efficiency η_i the application is as follows: find ~~Plot~~ the value of λ first on axis $z = 2$, proceed parallel to the next diagonal straight line until reaching the pertinent axis z (= 2, 3, 4, 6, 8, or ∞). Perpendicular over the intersection on the ordinate corresponding to the given loading, read the induced efficiency η_i at the parameter curves. It at the same time gives the axial efficiency η_a at the same ordinate in the left-hand portion on the horizontal asymptotes of the efficiency curves. The difference between η_a and η_i represents the losses due to slipstream twist and finity of blade number.

The straight lines plotted diagonally to axes z are not exactly parallel, but gradually straighten out with increasing coefficient of advance, as stipulated by figures 11 and 12. But, within the narrow range of customary coefficients of advance, these straight lines may be considered parallel. Then the transformation process on axes z can be simply replaced by a transparent scale with the points $z = 2, 3, 4, 6, 8, \infty$, which is horizontally placed over the chart so that its point $z = 2$ falls on the given coefficient of advance.

The gains in efficiency, obtainable by preservation of the remaining conditions through increase of the number of blades, are defined from points located on horizontal lines. On the other hand, a straight line of pitch 2 corresponds in figure 14 to the change in diameter at equal values of N = hp., n = r.p.m., ρ = density, v = flying speed, and z = number of blades, since the elimination of diameter D from

$$\lambda = \frac{v}{\pi n} \frac{1}{D} \tag{5.1}$$

and

$$c_l = \frac{N}{\frac{\rho}{2} \frac{\pi}{4} v^3} \frac{1}{D^2} \tag{5.2}$$

gives

$$c_l = \frac{8 \pi n^2 N}{\rho v^5} \lambda^2 \tag{5.3}$$

where the factor of λ^2 is Madelung's (reference 8) "geometric high speed." It contains only the given fixed quantities, is nondimensional and computable in logarithmic scale, for instance, by staking off with a divider. If this is effected on the vertical straight for $\lambda = 1$, the point defines the straight of pitch 2, on which the scale for diameter D can be marked according to equation (5.1). A reduction of diameter has an adverse efficiency effect, which may be overcome under certain circumstances by raising the number of blades.

This leads back to the question of "equivalent diameter" for different blade number previously touched upon in connection with the equivalence figures (section 2). Proceeding, for instance, from a 2-blade propeller for a certain condition of operation: On changing to 4 blades, the diameter is to be reduced while preserving the quantities appearing in the geometric high speed, so that the induced efficiency does not change. The construction is possible in either one of the charts and the results are identical: First, plot the point following from the given operating condition of the 2-blade propeller. Move horizontally to the left from this starting point so far as it corresponds to the transition from axis $z = 2$ to axis $z = 4$. From there, follow in correspondence to the diameter reduction along a straight line of pitch 2 to the intersection with the efficiency curve belonging to the starting point. The difference in height of the two curve points then indicates the ratio of the related loadings as well as the ratio of the squares of the coefficients of advance and the inverse ratio of the equivalent propeller disk areas.

According to the above, any degree of improvement in efficiency would be possible by suitable enlargement of diameter. But the adverse effect disregarded in the calculation caused by simultaneous approach of the propeller tip speed toward velocity of sound militates against this. It is therefore recommended that a constant tip speed be substituted for the constant flying speed v in the above arguments. The questions involved thereby are treated in an article by E. Bock and R. Nikodemus (reference 9), which follows.

REFERENCES

1. Betz, A.: Schraubenpropeller mit geringstem Energieverlust. Mit einem Zusatz by L. Prandtl. Nachr. der K. Gesellschaft der Wissenschaften zu Göttingen, Math.-phys. Kl. (1919), pp. 193-217. Abgedruckt in L. Prandtl und A. Betz, Vier Abhandlungen zur Hydrodynamik und Aerodynamik, Göttingen (1927), pp. 68-92.

2. Goldstein, S.: On the Vortex Theory of Screw Propellers. Proc., Roy. Soc., London. Vol. 123 (1929), pp. 440-65.

3. Betz, A., and Helmbold, H. B.: Zur Theorie stark belasteter Schraubenpropeller. Ingenieur-Archiv, Bd. 3 (1932), pp. 1-23.

4. Lösch, F.: Über die Berechnung des induzierten Wirkungsgrades stark belasteter Luftschrauben unendlicher Blattzahl. Luftf.-Forsch. Bd. 15 (1938) Lfg. 7, pp. 321-25. (See p. 1 of this Technical Memorandum.)

5. Helmbold, H. B.: Goldstein's Solution of the Problem of the Aircraft Propeller with a Finite Number of Blades. T. M. No. 652, N.A.C.A., 1931.

6. Lock, C. N. H., and Yeatman, D. M.: Tables for Use in an Improved Method of Airscrew Strip Theory Calculation. R. & M. No. 1674, British A.R.C., 1935.

7. Westwater, F. L.: Some Applications of Conformal Transformation to Airscrew Theory. Proc., Cambridge Philos. Soc. Bd. 32 (1936), pp. 676-84.

8. Madelung, G.: Beitrag zur Theorie der Treibschraube. DVL Jahrbuch, 1928, pp. 27-62.

9. Bock, G., and Nikodemus, R.: Die Aussichten des Luftschraubenantriebes für hohe Fluggeschwindigkeiten. Luftf.-Forsch. Bd. 15 (1938), Lfg. 7, pp. 334-39. (See p. 39 of this Technical Memorandum.)

LEGENDS

Figure 6.- Optimum circulation distribution $\underline{G}$ along the blade of the two-blade propeller (solid curves) compared to corresponding optimum distributions for finite blade number (dashed curves).

Figure 7.- Average factor $\kappa = \underline{G}^{(2)} : \underline{G}^{(\infty)}$; i.e., ratio of optimum circulation of 2-blade and infinite blade propeller for equal induced efficiency λ_i at the corresponding blade radii $r = R\,x$.

Figure 8.- Equivalence figure $\gamma_{31}^{(2)} = K_{31}^{(2)} : K_{31}^{(\infty)}$.
At light loading $(\eta_i \simeq 1)$, this is the ratio of c_s (or c_l) of the 2-blade propeller to the corresponding c_s (or c_l) of the equivalent infinite-blade propeller.

Figure 9.- Equivalence figure $\gamma_{52}^{(2)} = K_{52}^{(2)} : K_{52}^{(\infty)}$.

Figure 10.- Integral values K_{31} for $z = 2$ and $z = \infty$.

Figure 11.- Abscissas in mm (logarithmic scale with unit of 125 mm) corresponding to equal values $K_{31}^{(2)}$ and $K_{31}^{(\infty)}$. The second ordinate scale indicates the ratio $\lambda^{(\infty)} : \lambda^{(z)}$ of the "equivalent coefficients of advance" by high loading $(\eta \approx 1)$ to those for which equal c_s and c_l belong to different blade numbers ∞ and z at equal induced efficiency η_i.

Figure 12.- Abscissas for equal values $\left(K_{31}^{(2)} + K_{52}^{(2)}\right)$ and $\left(K_{31}^{(\infty)} + K_{52}^{(\infty)}\right)$. The second ordinate scale gives the ratio $\lambda^{(\infty)} : \lambda^{(z)}$ of the equivalent coefficients of advance by induced efficiency $\eta_i = 0.50$.

Figure 13.- Chart showing the relation between coefficient of advance λ, number of blades z, induced efficiency η_i, and the thrust loading c_s of the free-running optimum propeller.
Example: Given: $\lambda = 0.45$; $z = 4$; $c_s = 0.09$.
Read: $\eta_i = 0.950$; $\eta_a = 0.978$.

Figure 14.- Chart showing the relation between coefficient of advance λ, blade number z, induced efficiency η_i, and the power loading c_l of the free-running optimum propeller.

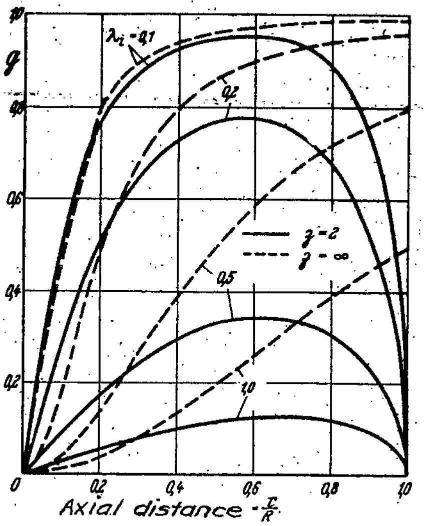

Figure 6.

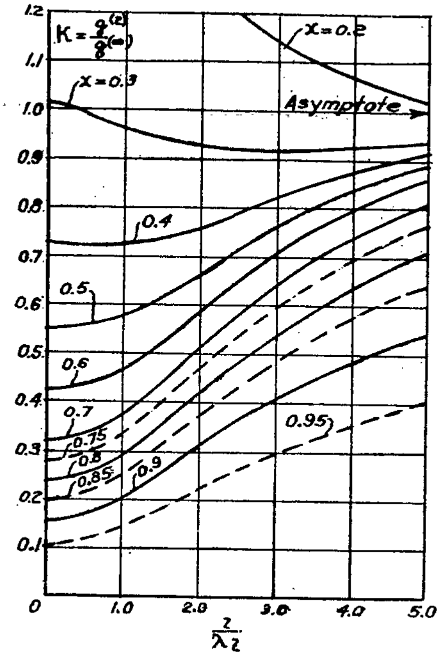

Figure 7.

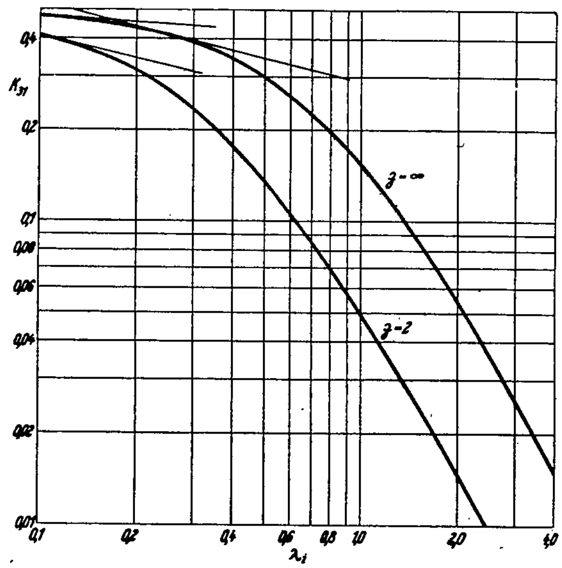

Figure 10.

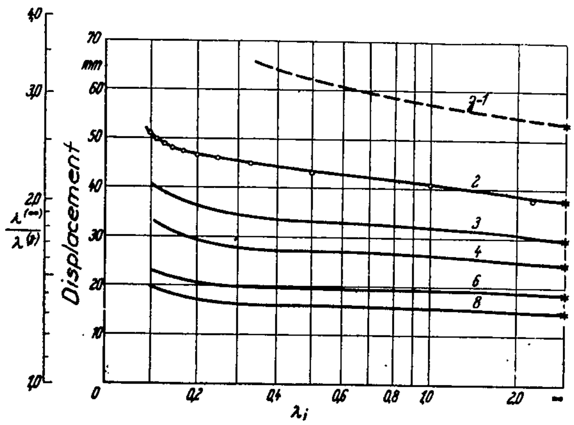

Figure 11.

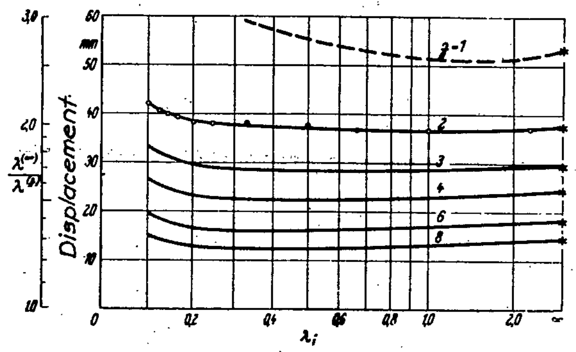

Figure 12.

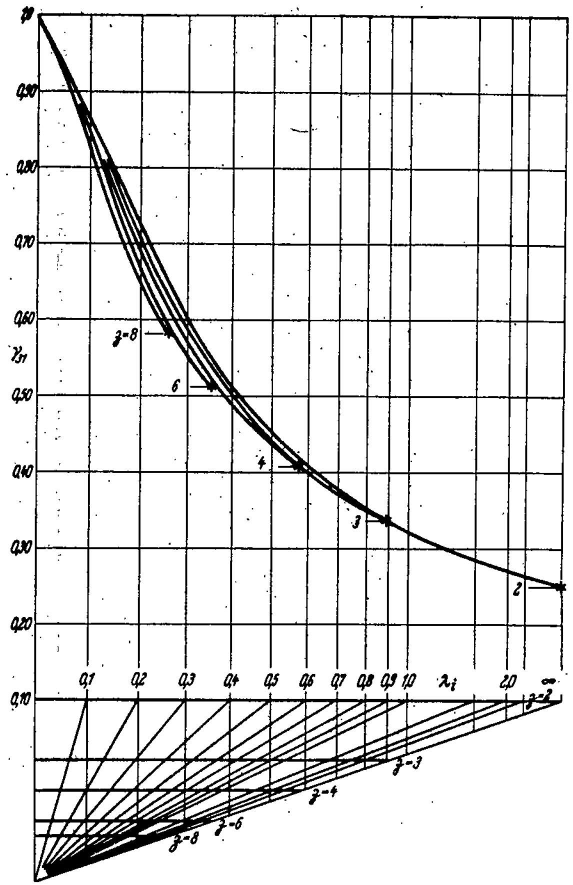

Figure 8.

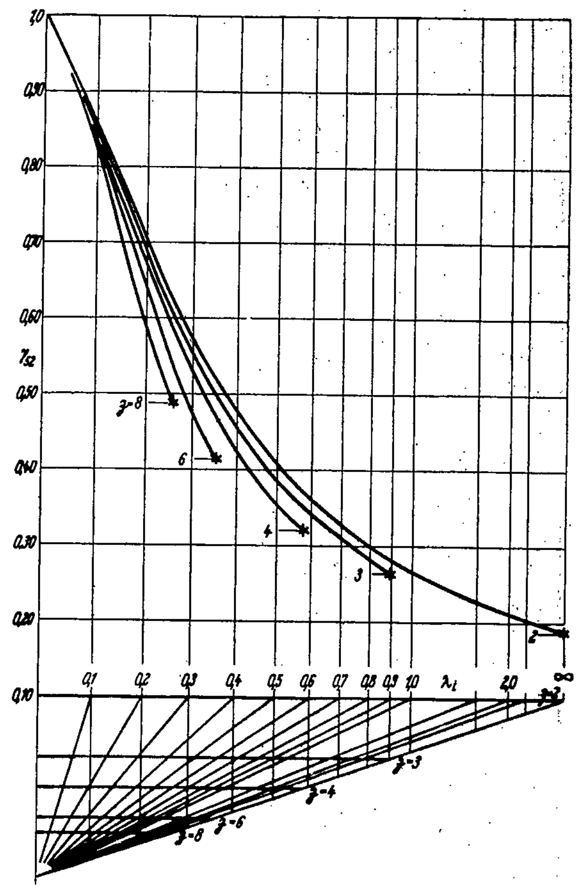

Figure 9.

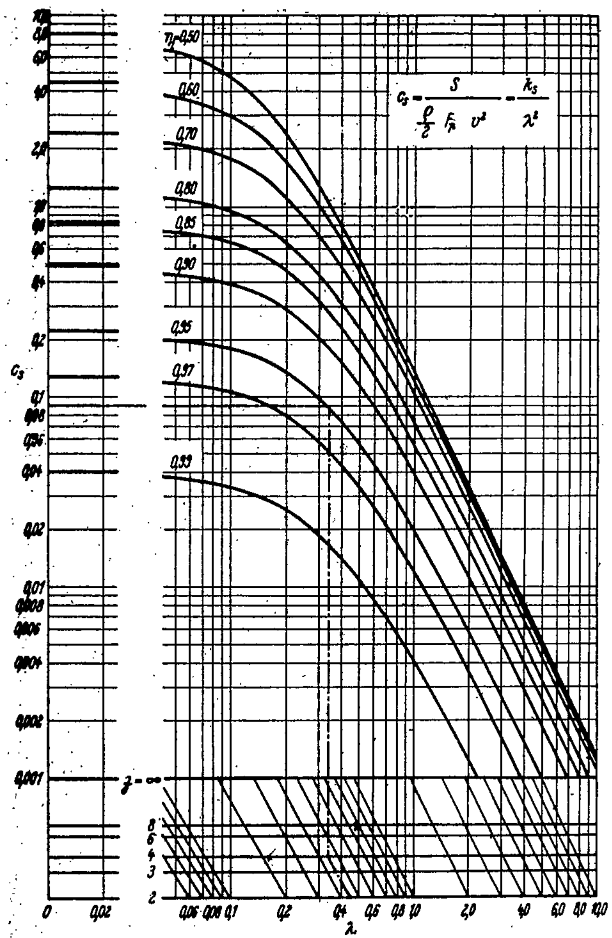

Figure 13.

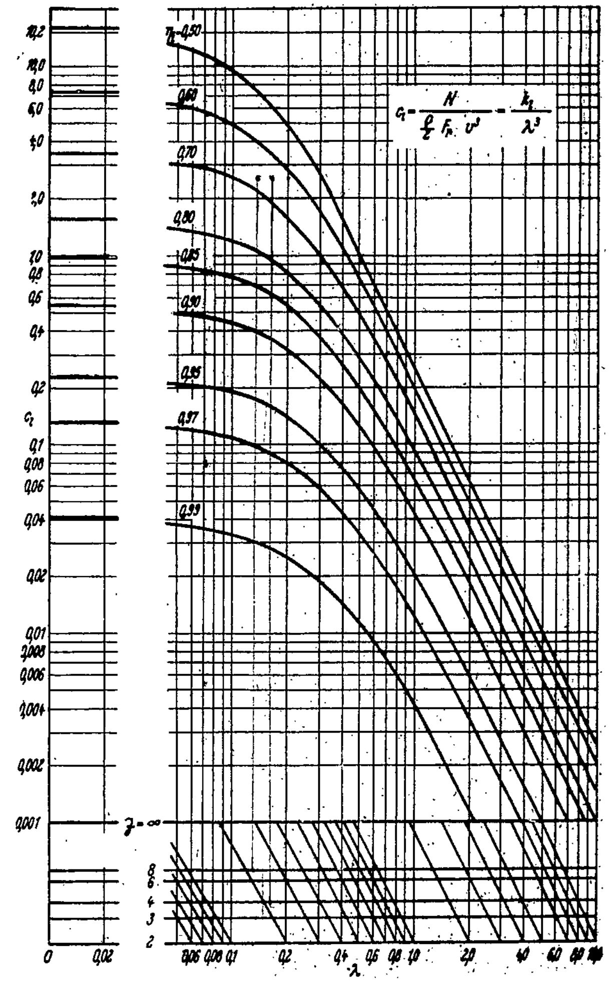

Figure 14.

$\frac{V}{\pi n D} = \lambda = .2073$

$B = Z = 4$

$P_c = C_\eta = 2.74$

PROSPECTS OF PROPELLER DRIVE FOR HIGH FLYING SPEEDS*

By G. Bock and R. Nikodemus

SUMMARY

Since the propeller efficiency becomes so much worse as the tip speed approaches sonic velocity and, to an increasing extent as the flying speed is higher, it is customary to keep the tip speed from exceeding 0.85 and 0.95 times the velocity of sound.

The induced efficiency η_i obtainable for certain flight conditions can be defined from ideal performance charts. The actual efficiency η_{th} of a free-running propeller contains in addition the efficiency-decreasing effect of the lift/drag ratio $\epsilon_p = \frac{c_w}{c_a}$, $\frac{C_{D_0}}{C_L}$ which, according to model propeller tests, ranges for modern propeller forms between 0.025 and 0.035 for optimum efficiency of high-speed flight.

The characteristic values of engine and propeller can be combined in a nondimensional quantity $\frac{(n^2 N/\rho)^{1/5}}{v_R}$, $= v_p$ termed the "high speed of the propeller tip." Together with the nondimensional flying speed $\frac{v}{v_R}$ ← tip speed, it defines the obtainable efficiencies.

The maximum efficiency at present flying speeds lies at around 600 to 700 km/h (373 to 435 m.p.h.); by further increase in flying speed, the efficiency drops materially, and so much more as v_p is greater and the number of blades is less (figs. 26 and 27).

The cause of the drop in efficiency at high flying speeds is ~~due to~~ the serious increase in twist losses (fig.

*"Die Aussichten des Luftschraubenantriebes für hohe Fluggeschwindigkeiten." Luftfahrtforschung, vol. 15, no. 7, July 6, 1938, pp. 334-339.

28). Whether these losses can be effectively lowered by counterrotating propellers or by guide surfaces, remains to be explained. $= \nu_p$

To lower the velocity of the propeller tip below the customary figure of 0.18 to 0.22 in order to effect an appreciable increase in propeller efficiency, involves substantially greater propeller diameters and considerably lower r.p.m. (fig. 29). The increased power plant and propeller weight connected herewith may make the gain in efficiency ineffectual.

1. INTRODUCTION

Increased flying speed has always been paramount in the development of the airplane. The criterion for the stage of development is seen from the world's speed records, shown in figure 15. Between 1918 and 1928, the speed rose from around 300 km/h (186 m.p.h.) to about 450 km/h (280 m.p.h.), or 50 percent; within the next 10 years, it rose to 700 km/h (435 m.p.h.) or another 80 percent. (In the meantime, the speed record for landplanes has been raised to 635 km/h (394 m.p.h.) by the Heinkel He 112.) In view of this steady progress, the temptation arises to make some predictions about future performances; speeds of 800 km/h and more are definitely feasible within the near future.

The purpose of the present article is to ascertain the propeller drive for such high flying speeds and what propeller efficiencies may be looked for. No propeller tests for such flying speeds being available at the present time, the arguments advanced here are, on the whole, based on theoretical considerations. This method has the advantage of greater general validity than investigations based solely upon measurements with certain propeller forms. Several simplifications are, of course, unavoidable.

2. EFFECT OF COMPRESSIBILITY OF THE AIR ON THE PROPELLER EFFICIENCY

As the velocity of flow approaches the velocity of sound, the drag of airfoils increases, as is known, considerably. The increase is, aside from the profile form, largely dependent upon the lift coefficient and begins to become very effective at Mach numbers of around 0.7 (fig. 16). On the propeller, the velocity with which the individual blade elements are contacted (fig. 17) is the resultant v_r of the velocity in circumferential direction u_r and the flying speed v. Consequently, there must be a distinct decrease in efficiency on approaching sonic velocity, when the resultant velocity v_r of a blade element starts to exceed the Mach number 0.7. This begins first at the blade tip $(v_r = v_R)$, although the decrease in efficiency connected with it is slight as long as this critical Mach's number remains confined to the tip regions themselves. The number of blade elements lying within adverse zone is largely dependent upon the flying speed, as seen in figure 17.

The resultant velocity of a blade element v_r is shown plotted against the distance $\frac{r}{R}$ from the axis of rotation for various v in figure 17, all velocities being referred to the propeller tip speed v_R. A scale has been added on the right-hand side by which, for instance, the tip speed v_R was made equal to 0.9 of the sonic velocity. It is found that, with increasing v while v_r remains the same, always more parts shift into the region of high Mach numbers. At the present maximum flying speeds of around $\frac{v}{v_R} = 0.6$ for a tip speed of $v_R = 0.9$ of velocity of sound, the outer third of the blade exceeds the critical Mach number of 0.7, while at a flying speed of $\frac{v}{v_R} = 0.8$, i.e., at around 835 km/h (518 m.p.h.) at 6 km (19,650 ft.) altitude, the entire blade length is within the advance zone. Consequently, the efficiency must decrease by increasing flying speed even if the same tip speed is maintained.

F. M. Thomas, F. W. Caldwell, and T. B. Rhines attempted to determine the change in efficiency on nearing sonic velocity in relation to the profile form, the angle of attack of the blade, or lift coefficient, respectively, as well as the coefficient of advance of the propeller on the basis of available test data (reference 1). They found that the efficiency decrease becomes less on approaching sonic velocity even for constant tip speed with increasing coefficient of advance, i.e., with increasing flying speed. This is in contradiction with the theoretical treatment cited above. Most likely, the data worked up by Thomas, Caldwell, and Rhines are insufficient for the separation of the individual effects in generally valid form, as Weinig's investigations (reference 2) also indicate.

Accordingly, since no satisfactory explanation of the efficiency decrease through approach of sonic velocity is possible, all velocities in the following study are, in order to minimize the error caused by omission of these influences, referred to the tip speed of the propeller, which at present usually ranges at Mach numbers of 0.85 to 0.95.

3. IDEAL PERFORMANCE CHARTS

Similarly to the method of dividing the drag of airfoil in induced and profile drag, the efficiency of a propeller can be divided into induced efficiency η_i and a quality factor ζ. The induced efficiency η_i allows for both the jet and twist losses, which in turn depend upon the coefficient of advance, blade loading and blade number (reference 3). Quality ζ is principally a function of the profile lift/drag ratio ϵ_p. As in the abbreviated airplane-performance calculation where the profile drag coeff. c_w is assumed constant (reference 4), the ϵ_p is figured as being constant. This method has the advantage, when establishing the efficiency curves, of not needing to know the blade forms, because the blades' areas do not enter into the calculations. The reliability of this method is discussed in detail in section 5.

The propeller efficiencies obtained from tests or theoretical studies are usually presented in charts, the coefficient of advance λ serving as abscissa and the performance factor k_l or the power loading c_l, respectively, as ordinate. A similar presentation was chosen by Kramer (reference 5, figs. 13 and 14) from which the induced efficiencies for any blade number and coefficient of advance are read. His efficiencies computed for $z = \infty$ and $z = 2$ blades are copied in figures 18 and 19, with logarithmic scales for abscissa and ordinate. This has the advantage of being able to read from the same diagram the performance figure k_l, the power loading c_l and the coefficient of advance, since these quantities are associated through $c_l = \frac{k_l}{\lambda^3}$. Similar charts are easily obtained for other blade numbers (reference 5, fig. 14).

4. EFFECT OF BLADE NUMBER ON THE EFFICIENCY

In the determination of the effect of blade number on the induced efficiency two fundamental cases must be distinguished: 1) The performance figure k_l may remain constant during the change to a different blade number, i.e., the propeller absorbs, independent of blade number, the same engine input by equal coefficient of advance, equal circumferential speed and equal diameter (cf. fig. 20, k_l = constant); 2) Under otherwise identical conditions the power input can increase in ratio to the number of blades $\left(\text{fig. 21, } \frac{k_l}{z} = \text{const.}\right)$.

In the first case, the increase in blade number improves the induced efficiency. The explanation for this is that the losses due to flowing around the blade tip become less for greater blade number because the helical areas induced by the propeller when passing through the air are closer together (reference 5). But, accompanying an increase in blade number with a corresponding blade loading $\left(\frac{k_l}{z} = \text{const., fig. 21}\right)$, the previously cited effect is counterbalanced by the rise in jet and twist losses produced as a result of increased blade loading. Under these conditions an increase in blade number has a detrimental effect on the efficiency. Because in comparative calculations based on model tests an increase in loading due to reduction of propeller diameter is frequently tacitly presumed, the generally accepted opinion is that an increase in the number of blades lowers the efficiency. For equal propeller diameter and equal input power and correct choice of blade form, the multiblade propeller must - as concerns efficiency - be always superior to the propeller with a few blades, provided the attainment of equal ϵ_p prevails for the multiblade propeller.

5. THE PROFILE LIFT/DRAG RATIO

In order to obtain the actual propeller efficiency presented in the performance charts, figures 18 and 19, the inclusion of the profile drag through introduction of quality factor ζ is necessary. Here the Bienen-Kármán approximate formula (reference 6) may be applied, according to which the quality is

$$\zeta = \frac{1 - 2\varphi\ \epsilon_p\ \lambda/\eta_i}{1 + \frac{2}{3}\ \psi\ \epsilon_p\ \eta_i/\lambda} \qquad (1)$$

φ and ψ being coefficients dependent upon coefficient of advance λ. Then the theoretical efficiency of the propeller is:

$$\eta_{th} = \eta_i\ \zeta$$

Figure 8 shows ζ plotted against the induced coefficient of advance $\lambda_i = \frac{\lambda}{\eta_i}$, ϵ_p serving as parameter.

To gain an insight in the existence of ϵ_p on actually constructed propeller, especially in the vicinity of the optimum efficiency value, various propeller test data were so evaluated as to afford a connection between η and ϵ_p, the latter were defined according to equation (1). As for example, the evaluation of a British test (reference 6) is shown in figure 23. The relative coefficient of advance $\frac{\lambda}{\lambda_o}$ was chosen as abscissa, λ_o denoting the coefficient of advance at which the thrust for the momentary blade setting H/D becomes zero. The ratio of η to η_{max} of the particular blade setting and the ϵ_p computed from the efficiencies served as ordinate. At the blade settings of high-speed flight in vicinity of the optimum efficiency, the ϵ_p lie between 0.025 and 0.035; the results from other propeller test data are similar.

The following calculations, devoted to optimum efficiencies only, were therefore carried out with $\epsilon_p = 0.03$.

6. THE HIGH SPEED OF THE PROPELLER TIP

The characteristic figures of an engine are the power N, the propeller shaft r.p.m. n, and the air density ρ. These quantities can be combined in a term $n^2 \frac{N}{\rho}$, which follows from the power equation

$$k_l = \frac{N}{\rho/2 \; \frac{\pi \, D^2}{4} \; u^3} \qquad (2)$$

when the propeller diameter D and the circumferential velocity u are eliminated through the relation

$$D = \frac{u}{\pi \, n} \quad \text{and} \quad u = \frac{v_R}{\sqrt{1 + \lambda^2}} \quad \text{(reference 7)}$$

It is:

$$(n^2 \, N/\rho)^{1/5} = (k_l/8 \, \pi)^{1/5} \frac{v_R}{\sqrt{1 + \lambda^2}} \qquad (3)$$

This expression has the dimension m/s. It is closely related to the mechanical velcoity developed by Madelung (reference 8). Since, as explained in section 2, the speed of the blade tip for the conventional airplanes of today fluctuates only little, it appears quite suitable as reference quantity. Then equation (3) gives in non-dimensional form,

$$\nu_p = \frac{(n^2 \, N/\rho)^{1/5}}{v_R} = (k_l/8 \, \pi)^{1/5} \frac{1}{\sqrt{1 + \lambda^2}} \qquad (4)$$

which depends only on the characteristic values of engine and propeller, and in the following is termed "high speed of the propeller tip."

For predetermined characteristic engine values and an assumed tip speed of the propeller v_R, the high speed

ν_p is quickly obtained from chart, figure 7. It ranges between 0.18 and 0.22 for the modern engines.

Choosing a certain flying speed $\frac{v}{v_R}$ referred to tip speed v_R, the relation

$$\frac{v}{v_R} = \frac{\lambda}{\sqrt{1 + \lambda^2}}$$

gives the coefficient of advance λ. For a certain ν_p then, equation (4) affords for each λ a certain power figure k_l, which is coordinated to a certain η_{th} or η_i, respectively. The efficiency curves in figures 25 to 28 were computed in this manner.

The "high-speed of the propeller tip" is related to the "speed-power coefficient"

$$C_s = v \left(\frac{\rho}{N\ n^2}\right)^{1/5} = \lambda(8 \cdot \pi/k_l)^{1/5} \tag{5}$$

of U. S. reports, by virtue of

$$\nu_p = \frac{(n^2\ N/\rho)^{1/5}}{v_R} = \frac{1}{C_s}\,\frac{v}{v_R} \tag{6}$$

Since the U. S. value C_s contains, besides the characteristic values of the engine, the flying speed v, it is less suitable as reference quantity for the present study than the "high speed of the propeller tip."

7. PROPELLER EFFICIENCY AT HIGH FLYING SPEEDS

Figure 25 shows the induced efficiencies plotted against the nondimensional flying speed v/v_R for $z = \infty$ blades and the high speed 0.15, 0.20, and 0.25. The flying speed v is given as added abscissa in case the flying speed v_R amounts to 290 m/s. This corresponds to a Mach number of around 0.9 at 6 km altitude where the sonic velocity a is approximately 320 m/s. The shape of the curves indicates a maximum of the efficiences, which lies about at the presently reached top speeds. Increasing the high speed of the propeller tip effects a vitiation of the efficiency over the entire speed range. The reason for this is that, for equal tip speed v_R and otherwise identical conditions, an increase in high speed involves an increase in r.p.m. and consequently a reduction in propeller diameter and in the volume of air grasped by the propeller. The efficiency decrease at high flying speeds makes itself felt especially vitiative at high speeds of propeller tips, because then the decrease starts so much sooner.

The finite blade number effects a further decrease in efficiency, as shown in figure 26. The effect of blade number increases with the high speed of the propeller tip and the flying speed. The greater decrease in efficiency at high flying speeds is attributable to the increasing flow around the outer parts of the propeller surfaces, which is particularly great at high coefficients of advance (reference 5).

The introduction of ϵ_p in the efficiency (fig. 27) effects primarily a parallel displacement of the efficiency curves. For the modern high speeds of propeller tips, the efficiency of a free running, 3-blade propeller amounts to at the most $\eta_{th} = 0.83$ for flying speed $v = 800$ km/h (497 m.p.h.), if the admissible tip speed is assumed at $v_R = 290$ m/s.

The optimum efficiency at $\eta_{th} = 0.87$ lies at a flying speed of about 550 km/h (342 m.p.h.). If it were possible at 800 km/h flying speed to reduce the high speed of the propeller tip to $\upsilon_p = 0.15$, a theoretical efficiency of $\eta_{th} = 0.91$, i.e., an 8 percent absolute efficiency improvement could be achieved. The importance of reducing the r.p.m. for high flying speeds while maintaining the tip speed is plainly observed.

A survey of the efficiency losses for the 4-blade propeller and $\upsilon_p = 0.20$ is presented in figure 28. The zone marked a indicates the losses due to profile drag; zone b, the losses due to finity of blade number. Zone c bordered by the induced efficiency η_i and the axial efficiency η_a

for the $z = \infty$ blades, is a criterion for the twist losses. They are chiefly responsible for the material decrease in efficiency at high flying speeds. Whether or not it is possible to effectively lower the twist losses in this zone by using counterrotating propellers or by proper guide apparatus, cannot be decided from theoretical investigations alone.

The propeller diameters D for certain characteristic engine values under the cited assumptions and flying speeds at $\upsilon_p = 0.15$ and 0.20 are given in figure 29. The tip speed was chosen at 290 m/s equivalent to an air density at 6 km and a Mach number of 0.9.

Then the assumption of an engine output N gives the engine r.p.m. for any high speed of the propeller tip υ_p. The propeller diameter follows after combining equations (2) and (4) as:

$$F_p = \frac{\pi D^2}{4} = \frac{N}{\rho} \frac{1}{4 \pi \upsilon_p^5 v_R^5 (1 + \lambda^2)} = \frac{N}{\rho} \frac{(v_R^2 - v^2)}{4 \pi \upsilon_p^5 v_R^5} \qquad (7)$$

or, if for the quoted quantities $(N, \rho, v_R, \upsilon_p)$ the r.p.m. is determined from υ_p,

$$D = \frac{1}{\pi n} \sqrt{v_R^2 - v^2} \qquad (8)$$

The propeller diameter decreases, as is seen in figure 29, with the flying speed. Its size is primarily governed by υ_p and N. For instance: the propeller diameter at 800 km/h flying speed and $\upsilon_p = 0.20$ is around 2.5 meters for a 1,000 hp. engine, but 4.5 meters for a 3,000 hp. engine, whereby the r.p.m. drops from 1,390 to 800 r.p.m. Reverting to a high speed of propeller tip of $\upsilon_p = 0.15$, which, according to figure 27, results in about 8 percent gain in efficiency the propeller diameter increases respectively to 5 and 9 meters by a decrease of r.p.m. to 680 and 390 respectively. The gain in efficiency due to lowering the υ_p can therefore, especially by great engine power, be neutralized by the increased weight of the propeller and of the reduction gear of the engine.

Translation by J. Vanier,
National Advisory Committee for Aeronautics.

REFERENCES

1. Thomas, F. M., Caldwell, F. W., and Rhines, T. B.: Practical Airscrew Performance Calculations. Roy. Aeron. Soc., October 1937.

2. Weinig, F.: Luftschrauben für schnelle Flugzeuge. Luftf.-Forsch. Bd. 14 (1937), Heft 4, p. 168.

3. Bienen, Th. and von Kármán, Th.: Zur Theorie der Luftschrauben. Z.V.D.I., Bd. 68 (1924), p. 1315.

4. Schrenk, Martin: Calculation of Airplane Performances without the Aid of Polar Diagrams. T.M. No. 456, N.A.C.A., 1928.

   Schrenk, Martin: A Few More Mechanical-Flight Formulas without the Aid of Polar Diagrams. T.M. No. 457, N.A.C.A., 1928.

5. Kramer, K. N.: Induzierte Wirkungsgrade von Best-Luftschrauben endlicher Blattzahl. Luftf.-Forsch. Bd. 15 (1938) Lfg. 7, pp. 326-33. (See p. 18 of this Technical Memorandum.)

6. Lock, C. N. H., Bateman, H., and Nixon, H. L.: Wind Tunnel Tests of High Pitch Airscrews (Part 1). R.& M. No. 1673, British A.R.C., 1935.

7. Bock, G.: Wege zur Leistungssteigerung im Flugzeugbau, Luftwissen, Bd. 4, Nr. 4 (1937) p. 104.

8. Madelung, G.: Beitrag zur Theorie der Treibschrauben. DVL-Jahrbuch, 1928, p. 27.

LEGENDS

Figure 15.- Rise of speed records.

Figure 16.- Effect of high flying speed on the profile drag (N.A.C.A. Report 492).

Figure 17.- a sonic velocity v flying speed
v_R tip speed; $v_r = (r/R)\ v_R$
u circumferential speed; $u_r = (r/R)\ u_R$

Figure 17.- Resultant velocities v_r against axial distance $\frac{r}{R}$.

Figure 18.- Induced efficiencies $(z = \infty)$.

Figure 19.- Induced efficiencies $(z = 2)$.

Figure 20.- Effect of blade number on induced efficiency for constant blade loading $(k_l = \text{constant})$.

Figure 21.- Effect of blade number on induced efficiency for constant blade loading $\frac{k_l}{z} = \text{constant}$.

Figure 22.- Quality of propeller according to Bienen and von Kármán.

Number of blades $z = 4$

Design pitch $\frac{H_o}{D} = 1.5\ (r = 0.7\ R)$

Blade width ratio $\frac{t}{D} = 0.0775\ (r = 0.7\ R)$

Thickness ratio $\frac{d}{t} = 0.11\ (r = 0.7\ R)$

η propeller efficiency
ϵ_p lift/drag ratio
λ_o coefficient of advance for zero thrust

Figure 23.- Propeller efficiencies and ϵ_p. (R.& M No. 1673, British A.R.C.).

Figure 24.- Chart for computing the high speed of the propeller tip $\upsilon_p = \frac{(n^2 N/\rho)^{1/5}}{v_R}$.

η_i induced efficiency
$v_R = \sqrt{u^2 + v^2}$, tip speed

N horsepower
n propeller r.p.m.
ρ air density

Figure 25.- Induced efficiencies against flying speed, $(z = \infty)$.

η_{th} theoretical efficiency $(\epsilon_p = 0.03)$
$v_R = \sqrt{u^2 + v^2}$, tip speed

N horsepower
n propeller r.p.m.
ρ air density

Figure 26.- Induced efficiencies against flying speed, $(z = \infty, 4, 3)$.

η_i induced efficiency
$v_R = \sqrt{u^2 + v^2}$, tip speed

N horsepower
n propeller r.p.m.
ρ air density

Figure 27.- Theoretical efficiencies against flying speed, $(z = \infty, 4, 3)$.

η_a axial efficiency
η_i induced efficiency
η_{th} theoretical efficiency
z blade number
ϵ_p lift/drag ratio

n propeller r.p.m.
N horsepower
ρ air density
$v_R = \sqrt{u^2 + v^2}$, tip speed
v flying speed

Figure 28.- Efficiency losses against flying speed $(z = 4)$.

Figure 29.- Propeller diameter in relation to flying speed.

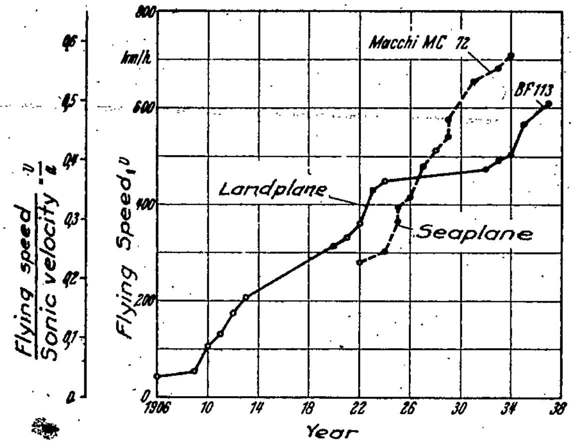

Figure 15.

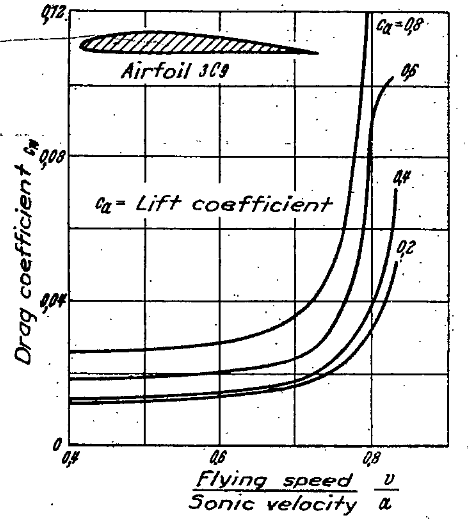

Figure 16.

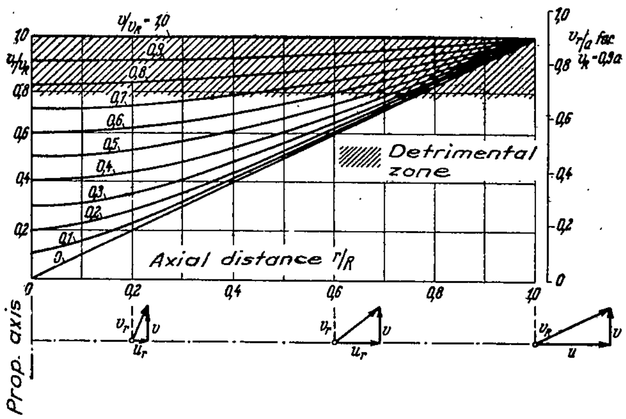

Figure 17.

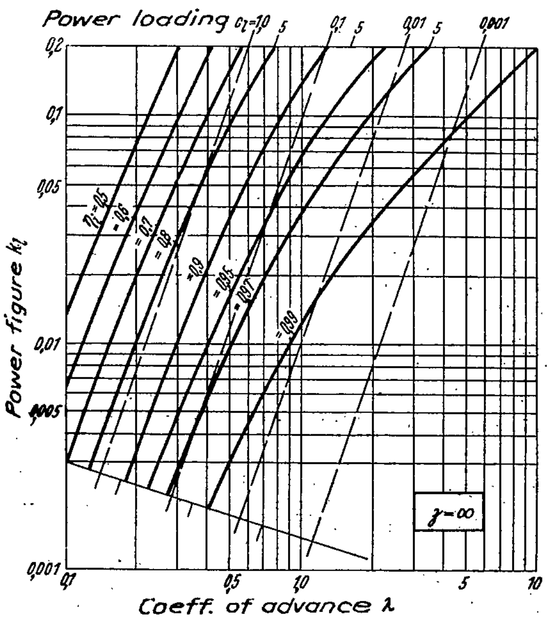

Figure 18.

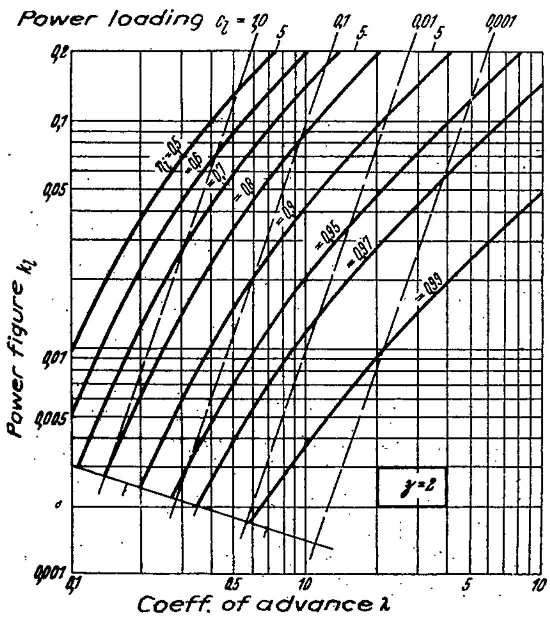

Figure 19.

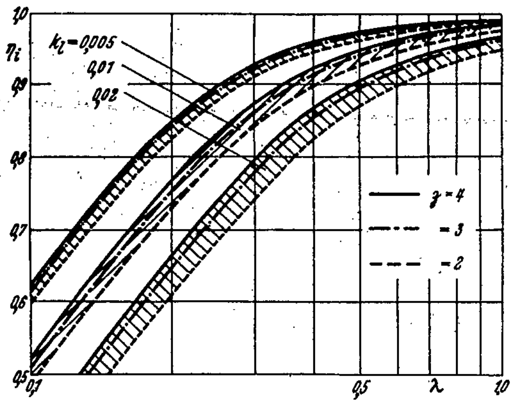

Figure 20.

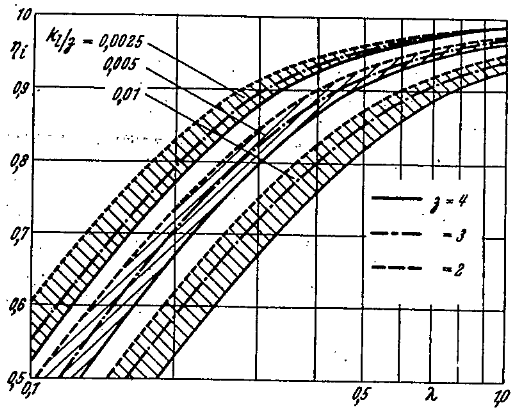

Figure 21.

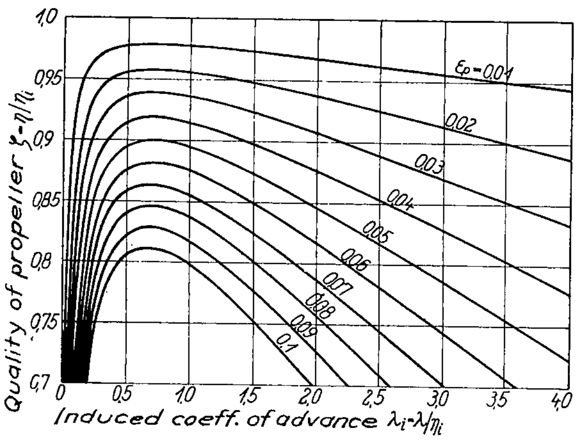

Figure 22.

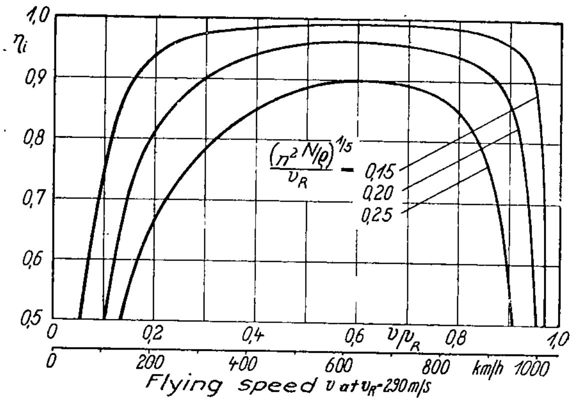

Figure 25.

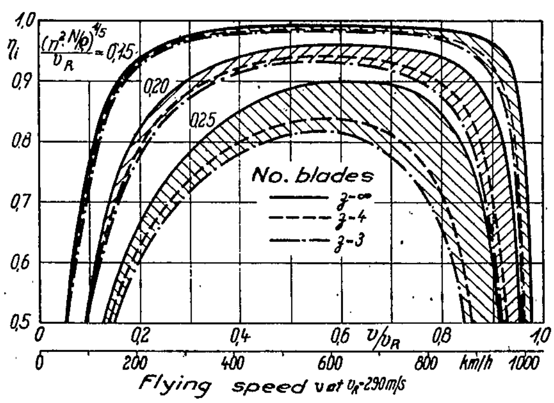

Figure 26.

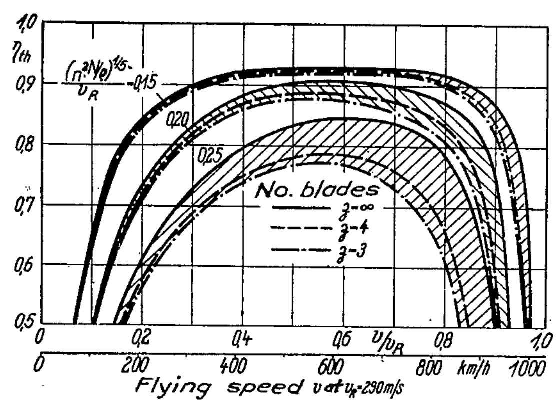

Figure 27.

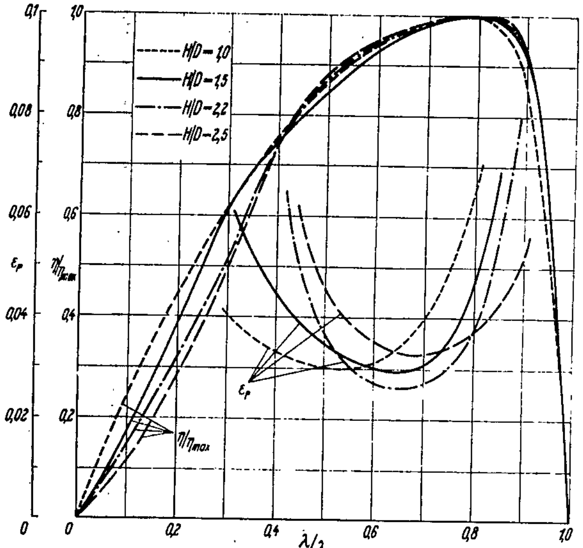

Figure 23.

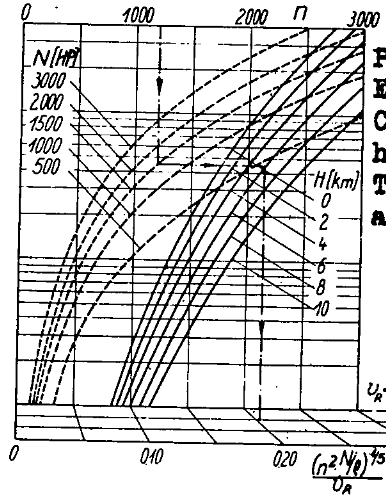

Example:
Propeller r.p.m.: 1200
Engine hp. 1500 hp.
Constant pressure height: 6 km.
Tip speed $v_R = 0.9a$
a = Sonic velocity

For it:

$$\frac{(n^2 N/\rho)^{1/5}}{v_R} = 0{,}203$$

Figure 24.

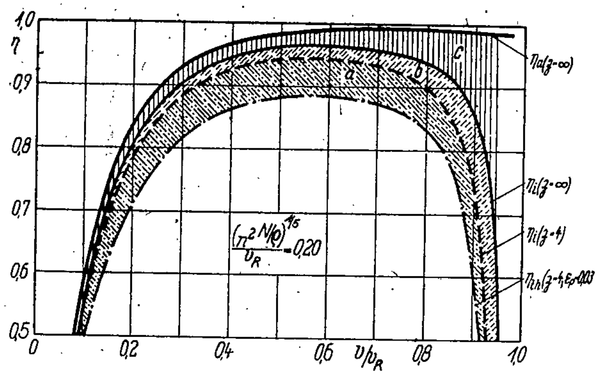

Figure 28.

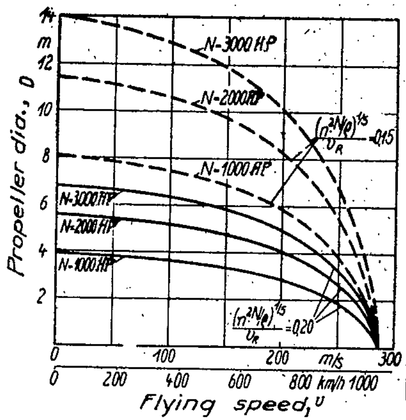

Altitude, H = 6 km.
Tip speed, $v_R = 0.9a = 290$ m/s
a = Sonic velocity
N = Engine hp.
n = Propeller r.p.m.
ρ = Air density

$\frac{(n^2 N/\rho)^{1/5}}{v_R}$	N,hp	r.p.m.
0,15	1000	680
·	2000	480
·	3000	390
0,20	1000	1390
·	2000	990
·	3000	800

Figure 29.